UNIVERSITY OF OKLAHOMA

GRADUATE COLLEGE

UTILIZING OBSERVATIONS AND CORAL RECONSTRUCTIONS TO ANALYZE THE VARIABILITY OF SEA SURFACE TEMPERATURES IN THE INTRA-AMERICAS SEA

A THESIS

SUBMITTED TO THE GRADUATE FACULTY

in partial fulfillment of the requirements for the

Degree of

MASTER OF SCIENCE

By

ALETHIA KIELBASA
Norman, Oklahoma
2024

Downloaded from SHAREOK. Persistent Handle URL: https://hdl.handle.net/11244/341262

UTILIZING OBSERVATIONS AND CORAL RECONSTRUCTIONS TO ANALYZE THE VARIABILITY OF SEA SURFACE TEMPERATURES IN THE INTRA-AMERICAS SEA

A THESIS APPROVED FOR THE
SCHOOL OF METEOROLOGY

BY THE COMMITTEE CONSISTING OF

Dr. Elinor Martin, (Chair)

Dr. Naoko Sakaeda

Dr. G.S. (Lynn) Soreghan

© Copyright by ALETHIA KIELBASA 2024
All Rights Reserved.

Acknowledgments

I would like to first thank my advisor Dr. Elinor Martin for her guidance and support throughout this project and for taking a chance on this former elementary school teacher. Her encouragement through my light bulb moments and even more so through my moments of uncertainty helped me get to this point. Though I may, at times, have wanted to be told what methods to use or what questions to ask, I am especially grateful that she supported me in a way that enabled me to grow as an independent thinker and researcher. I often think about how much I have grown as a researcher and how I approach research and community impacts of research. I greatly attribute this growth to Dr. Martin.

Thank you to my committee members, Dr. Naoko Sakaeda and Dr. Lynn Soreghan for their support as I worked towards the completion of my thesis and for providing invaluable perspectives and ideas on my research. I would also like to thank Dr. Kristine DeLong, Kylie Palmer, Nina Susich, and Gwendal Dolou at Louisiana State University for their contributions and expertise in all things corals. They provided some of the coral reconstructions and recalibrations used in this study. Additionally, I'd like to express my gratitude for the current and former members of the Climate Variability and Change group: Bryony Puxley, Melanie Shroers, Margaret Hollis, Gabriel Bromley, and Ben Davis. I also cannot omit Office 5700 which includes the CVC group but with a few very necessary additions: Andrea Gordon, Emily Tinney, Amanda Murphy, and Elisa Murillo. All of whom worked so hard to welcome me to the office and to foster a supportive, productive, hard-working, and hilarious working and learning environment for all who step inside.

I am fortunate to have the encouragement of friends and family in Oklahoma, South Florida, Indiana, Texas, South Carolina, California, and many more whose belief in me has propelled me forward through the trying and difficult moments. I would like to thank my parents and my two brothers for shaping me into the person I am today

and for showing me how capable I am through their support and encouragement. It was through this support that I had the confidence and motivation to pursue a difficult degree. Growing up with my brothers in a house full of love and consideration for our planet and for others is a main part of why I chose to research climate variability with the ultimate goal of increasing our understanding of climate change in order to benefit future generations.

Finally, without these two, I can certainly say my journey to this point would not have been full of the hope, laughter, and support that it was: Warren, my husband and life partner, and (arguably most importantly) Casanova, my bright, special, intelligent, and sweet cat. Without doubt or hesitation, they followed me to Oklahoma so that I could pursue this dream. In fact, in moments of self-doubt or second-thoughts, they listened and provided me with enough support so that I could continue this difficult journey. It is an incredible feeling to be in a partnership so full of mutual love, respect, and support.

I am eternally grateful to all who have been listed here and for the roles they have played in helping me reach this point in my academic and professional journeys.

This work was funded by the National Science Foundation grant AGS 2102970. I would like to acknowledge the CESM LENS2 and supercomputing resources provided by the IBS Center for Climate Physics in South Korea.

Table of Contents

Acknowledgments **iv**

List Of Tables **vii**

List Of Figures **viii**

Abstract **xii**

1 Introduction **1**

2 Data & Methods **7**
2.1 Observations 9
2.2 Coral Proxies 9
2.3 CESM2 LENS2 15
2.4 Analysis Methods 16

3 Climatological Variability of Sea Surface Temperatures in the IAS **19**
3.1 Variability of Sea Surface Temperatures 19
3.1.1 Long-Term Trends in SST 19
3.1.2 GOM and Caribbean Power Spectra 24
3.2 Springtime Sea Surface Temperature Anomaly Dipole 35
3.2.1 Atlantic Warm Pool 43

4 Discussion **48**
4.1 Sea Surface Temperature Variability in the IAS 48
4.2 Springtime Sea Surface Temperature Anomaly Dipole 50
4.3 Atlantic Warm Pool 52
4.4 Limitations and Future Work 53

5 Conclusions **56**

Reference List **59**

Appendix **63**
1 Appendix A 63

List Of Tables

2.1 Coral-based reconstructions used in this study. *Coral records from CoralHydro2k. **Multiple coral cores per site with different slopes and intercepts per core, within the ranges listed. 12
2.2 Observational and model data used in this study. 16

3.1 Annual SSTA trends in the GOM and Caribbean separated by data used and region. Boxes indicates the years used to compute the trends were 1887-2012. Years across each coral site were inconsistent. As such, the trends per coral site were calculated using the record length available for that particular coral. Units: °C per year. SSTA trends from each record were all found to be significant, except Dry Tortugas FMA, using linear regression and t-test, though the resulting p-values could be the result of the correlation between years and SSTAs being significant. Significance and trends were then calculated using a polyfit, though the significance of the resulting slopes and p-vales were the same. 22
3.2 Same as Table 3.1, for the spring months FMA. 22
3.3 Dipole occurrences per decade per coral location. Dipole index is calculated with each pairing combination of GOM and Caribbean coral sites. Common years were used for each pairing, in some cases only a few decades were available for the dipole calculation. 40
3.4 Dipole occurrence totals and per decade per data type. "SD" refers to standardized SSTAs and "SD DET" refers to standardized detrended SSTAs. Coral dipole calculation in this table was performed after interpolating and averaging coral records in each region, resulting in a different per decade value than Table 3.3. CESM dipoles found after averaging the first ten model members SSTAs. 41

List Of Figures

1.1 Idealized schematic of a springtime sea surface temperature anomaly dipole with cool SSTAs in the GOM and warm SSTAs in the Caribbean. 2

2.1 Map of previously used domains for each region from (Muñoz et al., 2010). These domains were not used in this study. 8
2.2 Map of the IAS domains used in this study: GOM in gray and the Caribbean in red. Coral sites in the GOM denoted by stars and coral sites in the Caribbean denoted by diamonds. Shapefiles used from Flanders Marine Institute (Flanders Marine Institute, 2018). 8
2.3 Timeseries of SSTs in the GOM: (top left) Flower Gardens, (top right) Dry Tortugas, and (bottom) Cuba. Error spread for Cuba was calculated using the slope and intercept error associated with the record and was plotted as SST. Standard deviation was used to find error spread for Dry Tortugas. Root mean square error was used for Flower Gardens. SSTAs were plotted for Dry Tortugas and Flower Gardens. 13
2.4 Timeseries of SSTs in the Caribbean: (left) Little Cayman, and (right) Guadeloupe. Error spread was calculated using the slope and intercept error associated with each coral record. Sr/Ca ratios for Tobago were not available at the time of this study. 14
2.5 Distribution of SST difference between the Caribbean and GOM across all months from 1870-2023 using (a) HadISST and (b) ERSST. Distribution of SST differences exceeding 2°C by month with January as index 0 and December index 11 using (c) HadISST, and (d) ERSST. 17

3.1 Composite of SST in the IAS across all months using (a) HadISST, (b) ERSST, and (c) CESM. SSTs are in ℃ per year from 1887-2012. 20
3.2 Composite of SSTA trends by grid point in the IAS during FMA using (a) HadISST and (b) ERSST. Squares correspond to the FMA SSTA trends at each coral location. Trends are in ℃ per year. 23
3.3 Spectral analysis of area-averaged, detrended, standardized SSTAs using HadISST for the (a) GOM and (b) Caribbean during FMA from 1887-2012. In panels a-b, the SSTAs (black-solid), red noise (red-solid), 95% (green-dashed) and 90% (orange) significance are shown. (c) Coherence squared between the GOM and Caribbean time series shown with 95% and 90% significance. (d) Phase relationship between the time series, only shown when coherence squared is significant at 95%. Phase difference is zero at the dashed line. 28
3.4 Same as Figure 3.2 except with coral reconstructions. 29

3.5 Spectral analysis of area-averaged, detrended, standardized SSTAs using HadISST for the (a) GOM and (b) Caribbean during JJA from 1887-2012. In panels a-b, the SSTAs (black-solid), red noise (red-solid), 95% (green-dashed) and 90% (orange) significance are shown. (c) Coherence squared between the GOM and Caribbean time series shown with 95% and 90% significance. (d) Phase relationship between the time series, only shown when coherence squared is significant at 95%. Phase difference is zero at the dashed line. 30
3.6 Same as Figure 3.4 except with coral reconstructions. 31
3.7 Spectral analysis of area-averaged, detrended, standardized SSTAs using HadISST for the (a) GOM and (b) Caribbean during NDJ from 1887-2012. In panels a-b, the SSTAs (black-solid), red noise (red-solid), 95% (green-dashed) and 90% (orange) significance are shown. (c) Coherence squared between the GOM and Caribbean time series shown with 95% and 90% significance. (d) Phase relationship between the time series, only shown when coherence squared is significant at 95%. Phase difference is zero at the dashed line. 32
3.8 Same as Figure 3.6 except with ERSST. 33
3.9 Same as Figure 3.6 except with coral reconstructions. 34
3.10 Detrended standardized FMA SSTAs and dipole years using HadISST from (a) 1870-2023 and (b) 1887-2012. Standardized SSTAs and dipole years from (c) 1870-2023 and (d) 1887-2012. In all panels, GOM (black-solid), Caribbean (red-dashed), and dipole years (circles) are shown. . . 35
3.11 Same as Figure 3.9 except with ERSST. 36
3.12 Same as Figure 3.9 except with coral reconstructions and only 1887-2012. 37
3.13 FMA SSTAs and dipole years using CESM2 LENS2 ensemble members 1-10 from 1887-2012 (a) detrended and (b) not detrended. SSTAs found for each ensemble member, then averaged together before finding the dipole index. Figure is used to compare average number of dipoles from 1887-2012 with other records, not to compare specific years of dipole occurrences. In all panels, GOM (black-solid), Caribbean (red-dashed), and dipole years (circles) are shown. 38
3.14 Composite of detrended standardized SSTAs in the IAS using HadISST from 1887-2012 during (top) dipole years, (middle) non-dipole years, and (bottom) composite difference with 99% confidence (gray dots) using a Monte Carlo test. 44
3.15 Same as Figure 3.13 except with ERSST. 45
3.16 Composite of detrended standardized SSTAs in the IAS using HadISST from 1887-2012 during (a) June-November, (b) JJA, (c) NDJ for (top) dipole years, (middle) non-dipole years, and (bottom) composite difference with 99% confidence (gray dots) using a Monte Carlo test. 46
3.17 Same as Figure 3.15 except with ERSST. 46

3.18 Composite of hurricane season-mean SSTs in the IAS from 1887-2012 using (a) HadISST and (b) ERSST during (top) dipole years, and (bottom) non-dipole years. Black contour at 28.5℃ and blue contour at 29.5℃. 47

A.1 Spectral analysis of area-averaged, detrended, standardized SSTAs using ERSST for the (a) GOM and (b) Caribbean during FMA from 1887-2012. In panels a-b, the SSTAs (black-solid), red noise (red-solid), 95% (green-dahsed) and 90% (orange) significance are shown. (c) Coherence squared between the GOM and Caribbean time series shown with 95% and 90% significance. (d) Phase relationship between the time series, only shown when coherence squared is significant at 95%. Phase difference is zero at the dashed line. 64
A.2 Spectral analysis of area-averaged, detrended, standardized SSTAs using ERSST for the (a) GOM and (b) Caribbean during JJA from 1887-2012. In panels a-b, the SSTAs (black-solid), red noise (red-solid), 95% (green-dahsed) and 90% (orange) significance are shown. (c) Coherence squared between the GOM and Caribbean time series shown with 95% and 90% significance. (d) Phase relationship between the time series, only shown when coherence squared is significant at 95%. Phase difference is zero at the dashed line. 65
A.3 Spectral analysis of area-averaged, detrended, standardized SSTAs using HadISST for the (a) GOM and (b) Caribbean during FMA from 1870-2023. In panels a-b, the SSTAs (black-solid), red noise (red-solid), 95% (green-dahsed) and 90% (orange) significance are shown. (c) Coherence squared between the GOM and Caribbean time series shown with 95% and 90% significance. (d) Phase relationship between the time series, only shown when coherence squared is significant at 95%. Phase difference is zero at the dashed line. 66
A.4 Same as Figure A.1 except with ERSST. 67
A.5 Spectral analysis of area-averaged, detrended, standardized SSTAs using HadISST for the (a) GOM and (b) Caribbean during JJA from 1870-2023. In panels a-b, the SSTAs (black-solid), red noise (red-solid), 95% (green-dahsed) and 90% (orange) significance are shown. (c) Coherence squared between the GOM and Caribbean time series shown with 95% and 90% significance. (d) Phase relationship between the time series, only shown when coherence squared is significant at 95%. Phase difference is zero at the dashed line. 68
A.6 Same as Figure A.3 except with ERSST. 69

A.7 Spectral analysis of area-averaged, detrended, standardized SSTAs using HadISST for the (a) GOM and (b) Caribbean during NDJ from 1870-2023. In panels a-b, the SSTAs (black-solid), red noise (red-solid), 95% (green-dahsed) and 90% (orange) significance are shown. (c) Coherence squared between the GOM and Caribbean time series shown with 95% and 90% significance. (d) Phase relationship between the time series, only shown when coherence squared is significant at 95%. Phase difference is zero at the dashed line. 70
A.8 Same as Figure A.5 except with ERSST. 71
A.9 Composite of detrended standardized SSTAs in the IAS using HadISST from 1870-2023 during (top) dipole years, (middle) non-dipole years, and (bottom) composite difference with 99% confidence (gray dots) using a Monte Carlo test. 72
A.10 Composite of detrended standardized SSTAs in the IAS using ERSST from 1870-2023 during (top) dipole years, and (bottom) non-dipole years. 73
A.11 Composite of hurricane season-mean SSTs in the IAS using HadISST during (top) dipole years, and (bottom) non-dipole years. Black contour at 28.5℃ and blue contour at 29.5℃. 73
A.12 Composite of hurricane season-mean SSTs in the IAS using ERSST during (top) dipole years, and (bottom) non-dipole years. Black contour at 28.5℃ and blue contour at 29.5℃. 74

Abstract

The Intra-Americas Sea (IAS) includes the Gulf of Mexico and Caribbean, regions relatively understudied in comparison to the larger Atlantic, considering their importance in moisture transport across the United States, Central and South America. The influence of the IAS on hydroclimate in these regions is substantial and has been connected to various processes including tropical storms, the springtime sea surface temperature anomaly dipole and the Atlantic warm pool. However, observational records are not long enough to fully understand variability in this region, particularly on decadal, multi-decadal, and longer timescales and can disagree on signals. A typical springtime dipole is noted by cooler sea surface temperatures in the Gulf of Mexico and warmer in the Caribbean and has been linked to precipitation anomalies in the eastern US and much of the Amazon region. In boreal summer, the Atlantic warm pool is a phenomenon marked by anomalously warm sea surface temperatures, critical for hurricane development. This study uses observations, coral-based reconstructions, and climate model data from the nineteenth to the twenty-first century to examine the variability of the springtime dipole in the IAS and how it impacts the Atlantic warm pool. Coral data was retrieved from CoralHydro2k with the addition of new records near Tobago, Cuba, and Flower Garden Banks. Each record found enhanced warming in the Caribbean compared to the GOM. The reduction of the Loop Current inhibits warm Caribbean SSTs from warming the GOM, a potential cause of this trend difference between regions. Power spectra analysis found significant periods in each region within the periodicities for El Niño Southern Oscillation and Pacific Decadal Oscillation, in agreement with previous studies. During dipole years, in which the average was approximately 4 per decade, warmer sea surface temperature anomalies dominate the IAS in the following summer months through the end of the Atlantic hurricane season. Following a springtime dipole, the Atlantic warm pool increases in extent and intensity when compared to non-dipole years. Non-dipole years display the

opposite pattern with cooler sea surface temperature anomalies dominating the IAS in the summer and hurricane season. Climate projections indicate an increase in intensity of weather events such as extreme precipitation, drought as well as enhanced Atlantic hurricane seasons, all of which are particularly impactful to coastal communities lacking adaptive and resilient infrastructure in the Intra-Americas Region. Through the use of observations, models and proxy data, a better understanding of the variability of sea surface temperatures in the IAS will help these regions prepare for a changing climate.

Chapter 1

Introduction

The Intra-Americas Sea (IAS), composed of the Gulf of Mexico (GOM) and the Caribbean Sea, is of considerable importance as it can provide insight into climate variability as well as impact weather conditions across the Intra-Americas Region including the Caribbean and parts of Central, North and South America (Glenn et al., 2015; González et al., 2017). For instance, the IAS has been connected to various processes and events including moisture transport, tropical storms, the Atlantic warm pool (AWP), the mid-summer drought and convective systems (Glenn et al., 2015). Considering the climate of the IAS acts as an indicator for climate change elsewhere, it is a rather understudied region. In fact, González et al. (2017) deems that the response to a changing climate in the Mesoamerican and Caribbean region could serve as a "blueprint" for other areas. González et al. (2017) also highlights the level of risk to coastal communities along the GOM and Caribbean, many of which lack climate-change-ready infrastructure, threatening the well-being of these communities. This insinuates the treatment of the IAS and surrounding areas as a guide for climate change influence, including not only how sea surface temperature (SST) changes but also the response of nearby communities and scientific agencies. Climate projections indicate an increase in intensity for weather events such as extreme precipitation and extreme drought as well as enhanced Atlantic hurricane seasons, all of which are especially impactful to communities in the Intra-Americas Region (Durán-Quesada et al., 2020).

It is well known the oceans play a major role in global and regional climate due in large part to its high heat capacity (Xu et al., 2021). Oceans also have a high thermal inertia which allows for the communication between the oceans and the atmosphere via latent and sensible heating (Deser et al., 2003). As such, SST influence makes the study of sea surface temperature anomaly (SSTA) variability important for the predictions of life-impacting weather and climate conditions.

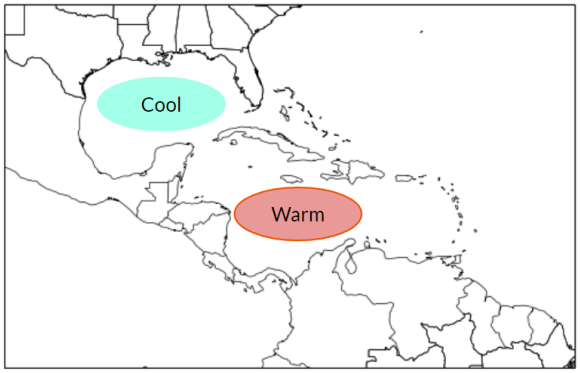


Figure 1.1: Idealized schematic of a springtime sea surface temperature anomaly dipole with cool SSTAs in the GOM and warm SSTAs in the Caribbean.

While each is part of the IAS, the GOM and the Caribbean can respond differently to remote impacts. An example of this is the springtime sea surface temperature anomaly dipole (SSAD) that forms in the IAS with cooler SSTAs in the GOM and warmer in the Caribbean (Figure 1.1).

The IAS is uniquely situated between two larger ocean basins (the Pacific and Atlantic), which drive SSTs in the GOM and Caribbean. GOM SSTAs are typically impacted by increased air-sea moisture differences, the Pacific Decadal Oscillation (PDO), and the Pacific North American (PNA) pattern while the Caribbean SSTAs are impacted in part by ENSO (Muñoz et al., 2010). In the springtime, the air-sea moisture differences in the GOM promote latent heat flux, cooling SSTs while increasing cloudiness, also contributing to cooler SSTs (Muñoz et al., 2010). The positive PNA phase

leads to a trough over eastern US, enhancing meridional flow and contributing to cooler SSTs in the GOM (Muñoz et al., 2010). During a warm ENSO phase, the subtropical jet is forced further south over the Caribbean, along with stronger eastward winds across the region. With this in mind, Muñoz et al. (2010) found a positive PNA in conjunction with a warm winter-to-spring ENSO phase leads to a SSAD with cooler GOM SSTAs and warmer Caribbean SSTAs. The PDO was found to be correlated with the GOM springtime SSTAs, though the impact of the PDO on the GOM differed depending on the strength of the warm ENSO and positive PNA phase (Muñoz et al., 2010). These teleconnections can lead to an anomaly dipole in the IAS during the spring that has its own variability worth studying.

Especially considering the depth to which summertime variability in the IAS has been examined, the springtime variability has been understudied. A study of the variability of the springtime dipole is also critical in the projection of future conditions and anomalous atmospheric circulations notably impacting precipitation in the Amazon basin, midwest United States, and the southeast United States (Muñoz et al., 2010). Muñoz et al. (2010) regressed precipitation anomalies with the SSAD index and found increased precipitation across the southeast United States and a decrease across the Midwest.

The Atlantic warm pool (AWP) is yet another prominent feature of the IAS climate system. The AWP is a body of water that is denoted by a SST of at least 28.5℃. In the summertime, the AWP reaches its maximum extent, extending across the Caribbean and GOM (Wang et al., 2008). The AWP is part of the larger Western Hemisphere warm pool (WHWP), separated by Central America. The complement to the AWP is the Eastern Hemisphere warm pool located in the Pacific; however, this study will focus on the AWP. Granted, Wang and Enfield (2001) found that the seasonal and interannual variability of SSTAs in the WHWP are not to the degree of larger processes,

such as ENSO; however, the high temperatures at which the SSTs in the WHWP vary have notable impacts on precipitation, convection and hurricanes. A warm AWP in the summer months has been found to increase available precipitable water and subsequently rainfall along the Gulf Coast and central and eastern United States (Wang et al., 2007).

IAS SST and springtime forcing impact the size of the AWP which, in turn, influences precipitation during the summer and the Atlantic hurricane season (Muñoz et al., 2010). For example, regions in and surrounding Central America experience a mid-summer drought of varying intensity each year, which economically impacts these areas. The NCAR Community Atmospheric Model has shown that an anomalously small AWP leads to an enhancement of this mid-summer drought (Wang et al., 2008) indicating a need for better prediction of summertime AWP features. Brocas et al. (2016) also found the climate in the IAS and tropical Atlantic during boreal summer is driven by the size of the AWP, thus implying the importance of predicting its size and intensity. Size of the AWP refers to the spatial extent of SST anomalies exceeding 28.5℃.

However, predicting the size of the WHWP and AWP is not a simple task. Enfield et al. (2006) determined the extent of the AWP is sometimes (and sometimes not) forced by El Niño events during boreal winter. Rather, prediction of AWP extent is a complicated process that includes consideration of SST anomaly persistence in the eastern Pacific accompanied by either a positive or negative North Atlantic Oscillation (NAO) phase (Enfield et al., 2006). Adding to the complexity, spring forcing in the IAS is potentially a key factor in determining the size and intensity of the proceeding summertime AWP (Enfield et al., 2006). As such, this study includes the examination of the relationship between the IAS SSAD and the AWP extent and intensity. These phenomena have been studied independently though, rather understudied given their

climatic importance, have not been explored in depth as two related phenomena. This study expands on the variability of the SSAD by examining how it has changed over the last 150 years. Considering global SSTs are increasing and a thirty-year warming trend in the GOM and Caribbean (Glenn et al., 2015) as well as a differing response to this trend by each region, it is expected the SSAD would become less symmetric as the springtime cooler temperatures in the GOM warm, resulting in a warmer summertime AWP.

Global climate models (GCMs) continue to show SST and precipitation biases in the IAS (Liu et al., 2012; Martin and Schumacher, 2012; Brotons et al., 2024). However, to accurately constrain these models, an improvement in SST data availability and reliability is necessary. Observational gridded data, while often longer record lengths than modern in-situ observations, experience non-systemic biases. To help improve climate predictability in the IAS, this study employs the use of GCM output, gridded SST data products, and coral proxy records.

Often overlooked as a source of SST variability data, particularly in the tropics, corals are uniquely situated to capture environmental conditions over time. Corals act as large biologic thermometers, keeping a record of SSTs dating back decades, if not hundreds of years. Due to their continuous annual growth, corals can provide generally uninterrupted data, depending on the coral species, at monthly and sometimes weekly resolutions (Corrège, 2006). SST can be reconstructed through the use of geochemical tracers that are measurable due to the corals' aragonite skeletons (Corrège, 2006). Massive corals, in particular, are used as they undergo fewer alterations over time such as erosion and breakage (Corrège, 2006). The relative ease at which coral cores are dated is yet another reason corals are useful climate proxies. Corals are dated through chemical dating (e.g. uranium and lead trace elements), counting density bands using X-radiographs, and historical event verification such as well-known flood events or

volcanic eruptions (Buddemeier et al., 1974; Corrège, 2006). While there are various tracers (e.g. δ^{18}O, Sr/U, Li/Ca, etc.) often employed as proxies for SST, this study focuses on Sr/Ca, as it is one of the most reliable and widely used proxies for SST. Though δ^{18}O is also widely used, often in conjunction with Sr/Ca particularly for sea surface salinity reconstructions, Sr/Ca is less variable in seawater than δ^{18}O, making it a reliable and easy to use tracer (Corrège, 2006).

Coral data is unique to the tropics and can provide valuable information about the region. Previous studies have used coral records to study SST variability and teleconnections in each basin in the IAS separately as well as extensively in the tropical Pacific. This study uses the most up to date coral records at the time of this study, in the GOM and CBN with improved coral site distribution, allowing for more reliable SST representations of the larger areas.

The goal of this study is to improve understanding of changes in SST over the past 150 years in each region of the IAS (Caribbean and GOM) and how the regions co-vary to help improve information available for extreme weather preparedness. To achieve this goal, the following objectives will be addressed:

Objective #1: Complete an extensive comparison of SST variability in the Gulf of Mexico and Caribbean over the past 125 and 150 years.

Objective #2: Assess and understand the mechanisms of variability of the spring-time sea surface temperature anomaly dipole in the IAS.

Objective #3: Evaluate and understand the relationship between the IAS spring-time sea surface temperature anomaly dipole and the summertime peak AWP.

Objective #4: Increase the SST record length in the region and improve the reliability of the results through comparisons between observations, coral proxies, and climate models.

Chapter 2

Data & Methods

Previous studies used the rectangular domains 12°- 20°N, 66°-88°W (Caribbean) and 22°-32°N, 76°-96°W (GOM) shown in Figure 2.1, (Muñoz et al., 2010) to define each region. However in this study, shapefiles for the GOM and Caribbean were utilized and obtained from Marine Regions (Figure 2.2) (Flanders Marine Institute, 2018). These shapefiles were applied to mask the areas of interest with more detail, allowing for better analysis of the SSTs in each marine region and inclusion of all coral record sites used in this study. Given the coarser resolution of gridded SST data, the masked areas were not as accurate along the coastlines. For all datasets, monthly anomalies were calculated by removing the seasonal cycle and then standardized.

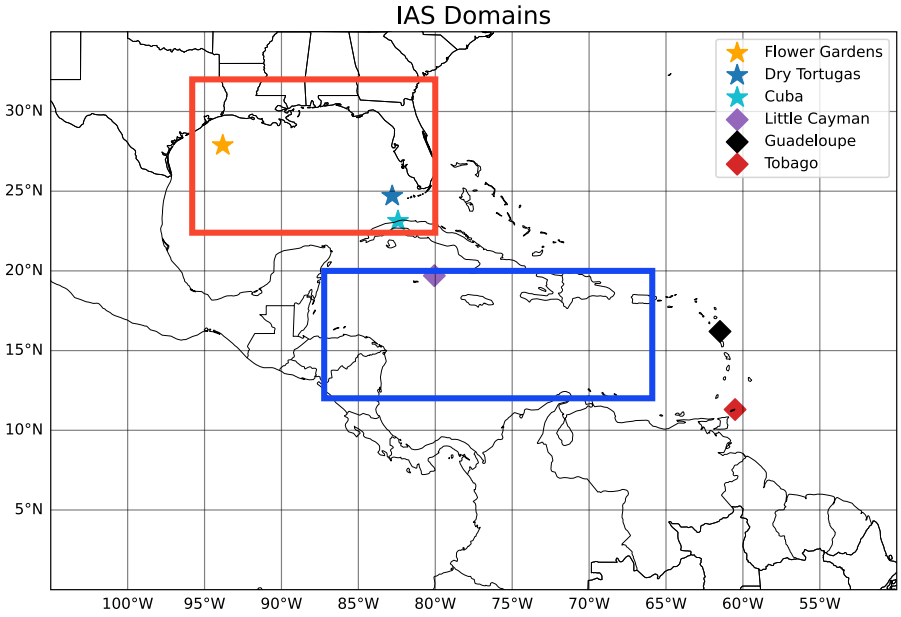


Figure 2.1: Map of previously used domains for each region from (Muñoz et al., 2010). These domains were not used in this study.

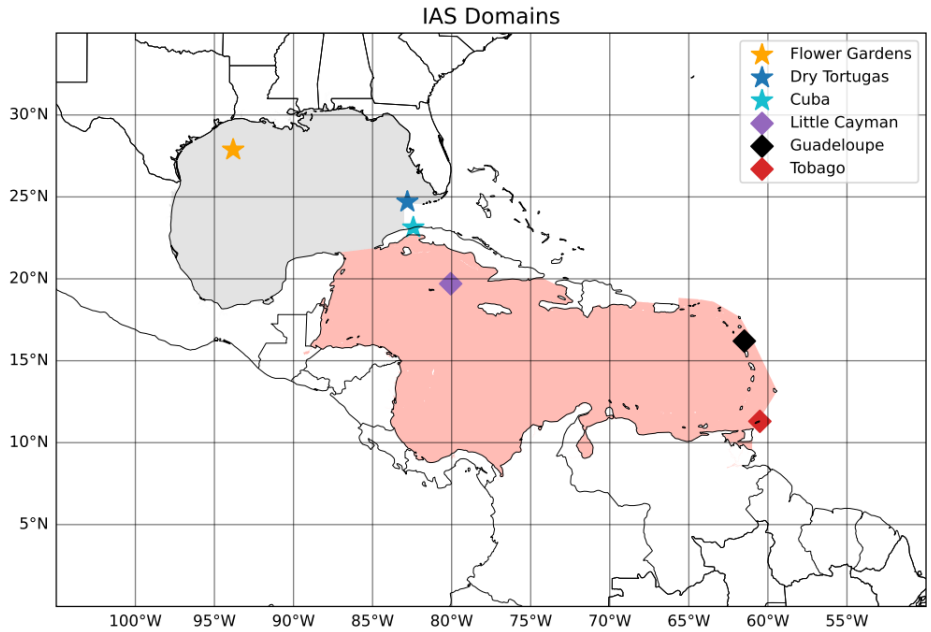


Figure 2.2: Map of the IAS domains used in this study: GOM in gray and the Caribbean in red. Coral sites in the GOM denoted by stars and coral sites in the Caribbean denoted by diamonds. Shapefiles used from Flanders Marine Institute (Flanders Marine Institute, 2018).

2.1 Observations

Reconstructed SST data for the GOM and Caribbean are from the Met Office Hadley Centre Sea Ice and Sea Surface Temperature (HadISST) dataset (Rayner et al., 2003) as well as the Extended Reconstructed Sea Surface Temperature (ERSSTv5) dataset (Huang et al., 2017) for observational intercomparison. HadISST is a collection of monthly global SST and sea ice concentrations on a 1° latitude-longitude grid from 1870 up until the present. In HadISST, the SSTs were reconstructed using an EOF technique, reduced-space optimal interpolation along with incorporated in-situ observations (Rayner et al., 2003). To reduce gaps in coverage, data were compiled from several sources including the Met Office Marine Data Bank, the Global Telecommunications System, and the Comprehensive Ocean-Atmosphere Data Set. HadISST is used due to its global coverage as well as its substantial timescale (150 years), providing enough data to portray SST variability in the GOM and Caribbean.

ERSST global monthly SSTs are on a 2° latitude-longitude grid from 1854 up until the present. In ERSST, the SSTs were reconstructed using ship and buoy SST data from the International Comprehensive Ocean-Atmosphere Dataset (ICOADS), Argo Float GDAC data, and ice concentrations from HadISST (Huang et al., 2017). The datasets used to reconstruct SSTs in ERSST were updated in version 5 in addition to improvements in reliability of spatial variability of SSTAs, particularly useful for regional climate studies such as this one (Huang et al., 2017).

2.2 Coral Proxies

The coral-based reconstructions used in this study were obtained, in large part, from the CoralHydro2K database, a curated and growing collection of coral proxies including δ^{18}O and Sr/Ca (Walter et al., 2023). CoralHydro2k seeks to provide an easily

accessible database of temporally long hydrological and temperature records in order to better understand the impacts of anthropogenic climate change (Walter et al., 2023). This study utilizes Sr/Ca proxies for SST in the GOM and the Caribbean. A total of three coral sites were used in the GOM: Dry Tortugas, Northwest Cuba, and Flower Garden Banks (Figure 2.2). Similarly, three coral sites were used in the Caribbean: Little Cayman, Guadeloupe, and Tobago (Figure 2.2). The Dry Tortugas, Little Cayman, and Guadeloupe records were obtained from CoralHydro2k (Walter et al., 2023; Flannery et al., 2017, 2018; Flannery and Poore, 2013; Weinzierl et al., 2016; Hickey et al., 2013; DeLong et al., 2016, 2014, 2011; von Reumont et al., 2018, 2016; Hetzinger et al., 2010, 2006). The Cuba, Tobago and Flower Gardens records were not yet submitted to be included in the CoralHydro2k database. The Cuba and Tobago records were obtained from PANGAEA (Harbott et al., 2023) and NOAA NCEI (Ong et al., 2022). Finally, the Flower Gardens data was provided by a research group from LSU. The total record length for the GOM and the Caribbean is 1733-2012 and 1887-2012 respectively. Further information regarding the records used can be found in Table 2.1.

Sr/Ca ratios were converted to SST using linear regression calibration equations unique to each coral species and location.

$$Sr/Ca = m \times SST + b \tag{2.1}$$

Sr/Ca and SST are inversely related: lower Sr/Ca means higher SST and vice versa. Equation 2.1 shows the linear regression equation used for the Sr/Ca to SST conversion, where m is the slope and b is the y intercept of a particular coral species. Given Sr/Ca values through coral sampling, and the derived slope and intercept values, SST was calculated. The calibration equations for each coral were obtained from CoralHydro2k or the respective publications. These equations are calculated by regressing monthly

Sr/Ca and monthly observations (in situ, HadISST, ERSST, or OISST depending on the coral record length and location). Regression analysis methods often used include ordinary least squares, reduced major axis, and weighted least squares. The various methods used to convert to SST and calculate error in reconstructions made preparation of coral data for this study challenging. Figures 2.3 and 2.4 show the calculated error spread compared to SST and SSTAs. Limitations from availability of data led to the use of various error methods including RMSE, standard deviation, and slope and intercept error. As such the error spreads between records cannot be compared directly, however these plots demonstrate the general spread in SST and SSTA apparent in coral-based SST reconstructions.

Table 2.1: Coral-based reconstructions used in this study. *Coral records from Coral-Hydro2k. **Multiple coral cores per site with different slopes and intercepts per core, within the ranges listed.

Location	**Years**	**Chemistry**	**Core Code/IDs**	**Species**	**Slope**	**Intercept**
Dry Tortugas	1733-2012	Monthly Sr/Ca	FL17DTO01-02**	*O. faveolata, S. siderea*	-0.043, -0.0392	10.11, 10.205
			FL18DTO01-04*		-0.049	10.46
			DE14DTO01-04**		-0.044, -0.041	10.06, 10.14
NW Cuba	1845-2005	Monthly Sr/Ca	CIM_C_2-2-1	*S. siderea*	-0.045	10.35
			CIM_C_2-2-2			
Flower Garden Banks	1751-2004	Monthly Sr/Ca	05WFGB3	*S. siderea*	-0.043	9.96
Little Cayman	1887-2012	Monthly Sr/Ca	RE18CAY01*	*D. strigosa*	-0.0386	10.023
Guadeloupe	1895-1999	Monthly Sr/Ca	HE10GUA01*	*D. strigosa*	-0.063	10.57
Tobago	1988-2016	Monthly Sr/Ca	SPEY1	*S. siderea*	-0.072	10.79

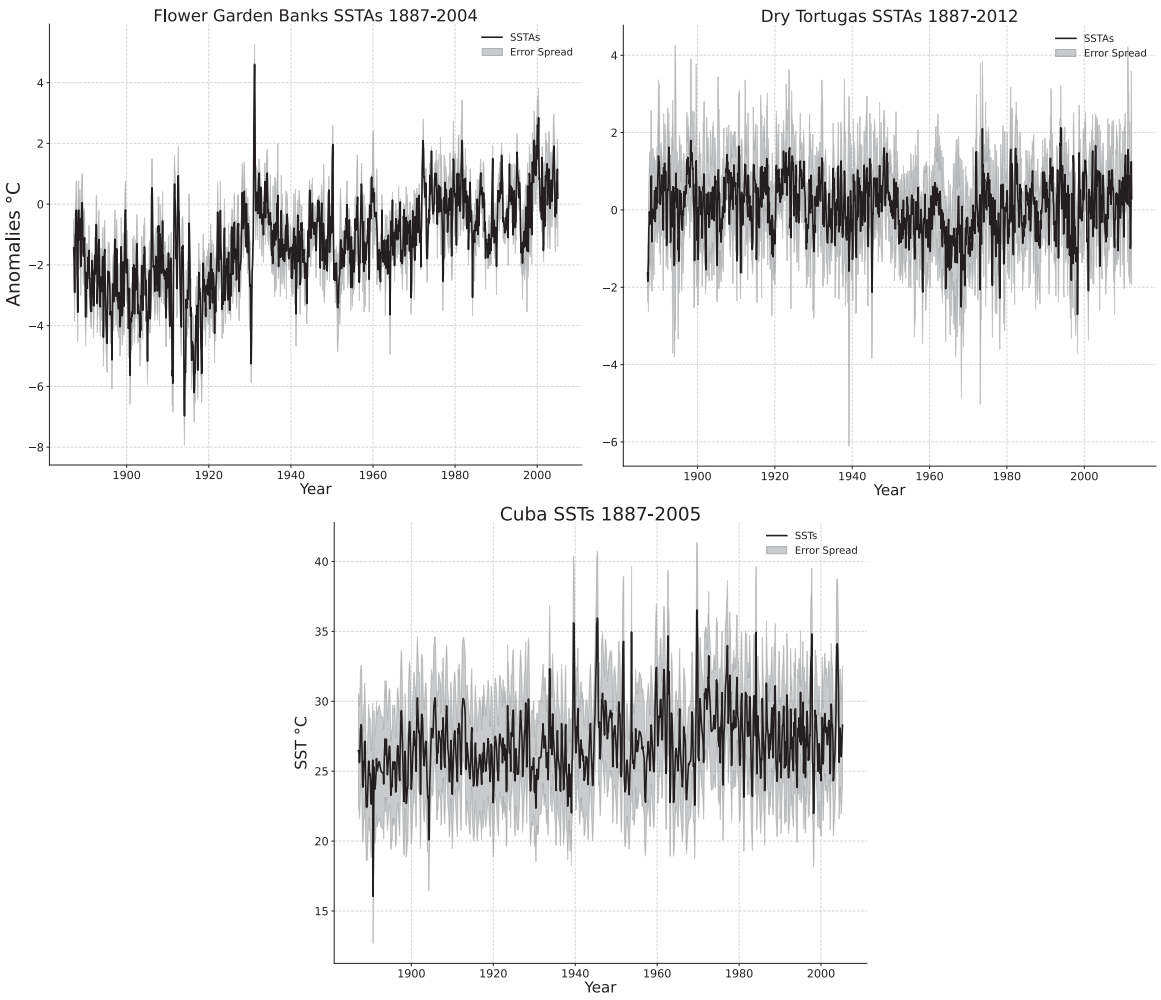


Figure 2.3: Timeseries of SSTs in the GOM: (top left) Flower Gardens, (top right) Dry Tortugas, and (bottom) Cuba. Error spread for Cuba was calculated using the slope and intercept error associated with the record and was plotted as SST. Standard deviation was used to find error spread for Dry Tortugas. Root mean square error was used for Flower Gardens. SSTAs were plotted for Dry Tortugas and Flower Gardens.

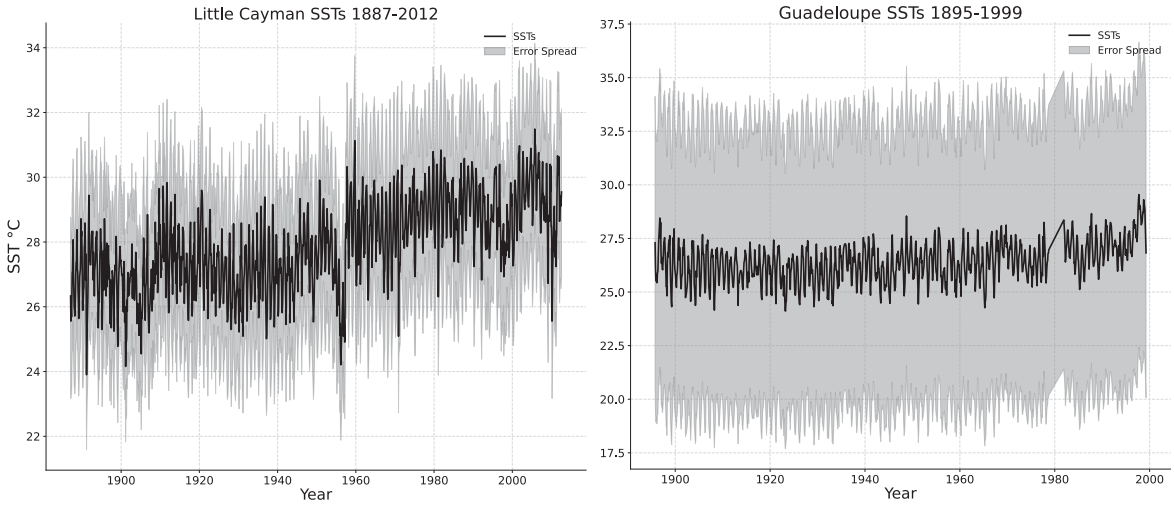


Figure 2.4: Timeseries of SSTs in the Caribbean: (left) Little Cayman, and (right) Guadeloupe. Error spread was calculated using the slope and intercept error associated with each coral record. Sr/Ca ratios for Tobago were not available at the time of this study.

2.3 CESM2 LENS2

The Community Earth System Model (CESM2) Large Ensemble Community Project (LENS2) was used for the model component of this study. LENS2 consists of a 100-member ensemble spanning the years 1850-2100 at 1° spatial resolution (Rodgers et al., 2021). For the purposes of this study, ensemble members one through ten (to be expanded to all members in future work), and only the years 1887-2012 were used in order to compare common years across all data. These ten members begin at 20-year intervals beginning at 1001 and are initialized with the Coupled Model Intercomparison Project (CMIP6) biomass burning forcing (Rodgers et al., 2021). Table 2.2 shows a comparison of the model and observational SST datasets.

Table 2.2: Observational and model data used in this study.

Data	Years	Temporal/Spatial Resolution	Data Type
HadISST	1870-2023 1887-2012	Monthly 1° x 1°	Observations
ERSST	1870-2023 1887-2012	Monthly 2° x 2°	Observations
CESM LENS2	1887-2012	Monthly 1° x 1°	Model

2.4 Analysis Methods

Addressing the second objective, years where a dipole is present were identified by creating an index utilizing the method described by (Muñoz et al., 2010), with slight alterations:

- Used shapefiles for the GOM and the Caribbean as opposed to rectangular areas
- Included dipole months February and April in addition to March as these months experience the largest SST difference between the GOM and Caribbean as well as accommodate potential errors in coral date conversions to units of time
- Defined a dipole as any instance the difference in standardized SSTAs between the Caribbean and GOM was greater than zero

Figure 2.5a and 2.5b show the distribution SST differences between the GOM and the Caribbean. The SSAD is noted by cool GOM anomalies and warm Caribbean anomalies. As such, positive SST difference values were targeted in order to determine the months of greatest SSTA difference. Figure 2.5c and 2.5d show the distribution of SST differences exceeding 2°C. HadISST and ERSST both found February, March, and

April (FMA) to be the months where the differences exceed 2°C at higher frequency than the rest of the year, which considers the addition of February and April in the SSAD, whereas Muñoz et al. (2010) included only March. Generally, the IAS dipole reaches a maximum in the spring with positive SSTAs in the Caribbean and negative SSTAs in the GOM; as such, standardized SSTAs were calculated for the months found to have the largest SST difference between the regions.

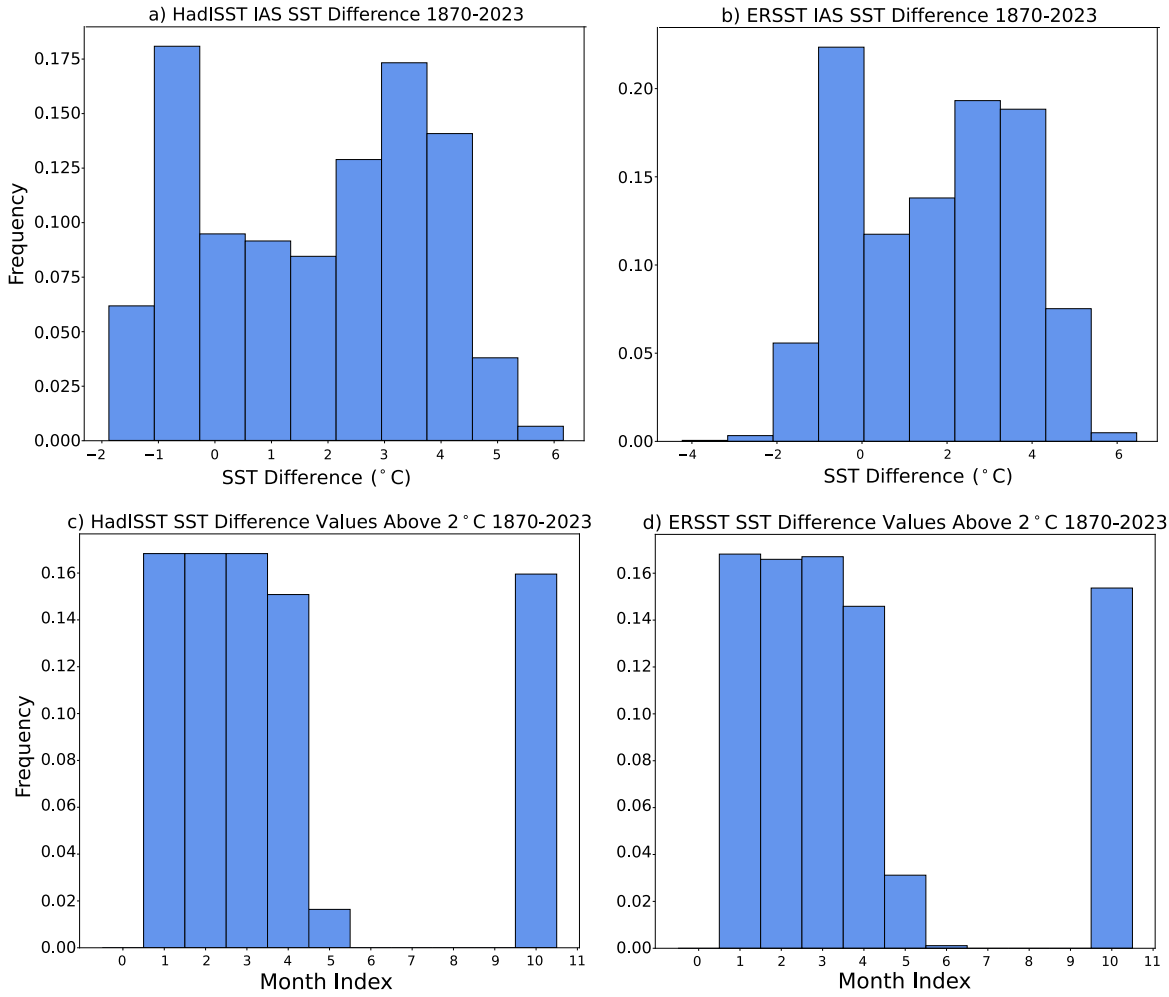


Figure 2.5: Distribution of SST difference between the Caribbean and GOM across all months from 1870-2023 using (a) HadISST and (b) ERSST. Distribution of SST differences exceeding 2°C by month with January as index 0 and December index 11 using (c) HadISST, and (d) ERSST.

These months were averaged together to get the average spring SSTA per year. Two record lengths were used: 1887-2012 and 1870-2023 depending on the dataset used, with 1887-2012 being the common years across all records and 1870-2023 common across observational data. Muñoz et al. (2010) also found via chi-square statistic, the GOM and the Caribbean are not independent but are oppositely related. The SSAD index was then constructed by calculating the difference between Caribbean SSTAs and GOM SSTAs in FMA. Dipole years were present where the difference value was greater than zero with non-dipole years at difference values less than or equal to zero. The dipole index was then populated with difference values greater than zero, omitting the rest. The difference values less than or equal to zero formed the non-dipole index. For the purposes of this study, non-dipoles or non-dipole years refer to either the opposite SSTA setup as the springtime dipole with anomalously warm GOM and cool Caribbean or no dipole present with equal anomalies in each region.

In an effort to examine the impact of the SSAD on the AWP, the dipole index was used to generate composites of SSTAs and SSTs during the months FMA, JJA, June-November, and NDJ for both, dipole and non-dipole years. These composites cover the domain of the entire IAS to compare the variability of SSTAs during hurricane season when the previous spring exhibited a dipole with springs that did not display a dipole.

Chapter 3

Climatological Variability of Sea Surface Temperatures in the IAS

3.1 Variability of Sea Surface Temperatures

3.1.1 Long-Term Trends in SST

Examining the variability of SSTs and SSTA trends in the GOM and the Caribbean provides insight into how these regions are varying and whether or not they are co-varying. Figure 3.1 shows average SSTs in the IAS from 1887-2012 for each gridded data type (HadISST, ERSST, CESM). There is agreement across records that warmest SSTs are generally located on the west coast of Mexico and Central America. The Caribbean is warmer on average than the GOM with CESM showing warmer SSTs than HadISST and ERSST. The first ten CESM2 LENS2 ensemble members do not show a cold bias in the IAS that has been seen in other studies (Figure 3.1c).

SSTAs were used to compare trends across observational data, coral-based reconstructions, and model data. Table 3.1 includes warming trends across all months in each coral location, the average across all coral sites, HadISST, ERSST, and the average trend from the first ten CESM2 LENS2 members from 1887-2012 (as well as 1870-2023 for the observational data). It is clear from the 1887-2012 averaged trends across all data types that the Caribbean is warming at a faster rate than the GOM

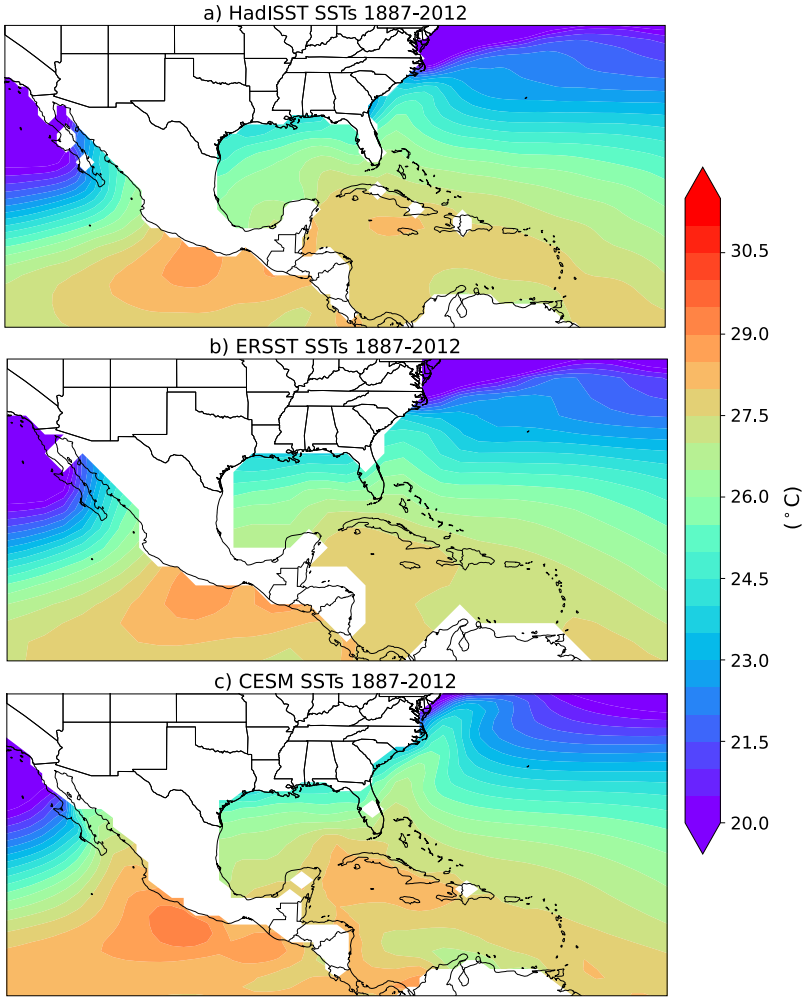


Figure 3.1: Composite of SST in the IAS across all months using (a) HadISST, (b) ERSST, and (c) CESM. SSTs are in ℃ per year from 1887-2012.

with trends ranging from 0.00056-0.0059 ℃ per year. Additionally, with the exception of the Guadeloupe coral reconstruction, individual coral sites located in the Caribbean indicate a warming rate greater than the GOM. When considering HadISST data over an increased record length, 1870-2023, the warming trend increases by 0.0004 ℃ per year in the GOM and decreases 0.0001 ℃ in the Caribbean. However, ERSST shows a rather drastic decrease in SSTAs when increasing the record length to 1870-2023. The average of the first ten members of CESM2 LENS2 demonstrate the lowest warming

trends in each region when compared to HadISST, ERSST, and the average of coral records. These trends are lower than those found in previous studies, though they utilized different data with shorter record lengths and different spatial domains (Glenn et al., 2015; Duan et al., 2021).

Table 3.2 exhibits the same trend information, but for the months FMA, when the SSAD is present. Again, there is an apparent difference in warming trends between the GOM and the Caribbean, with greater trends in the Caribbean. The springtime SSTAs in the GOM and Caribbean have larger warming trends than the overall annual trends. Each individual coral site also shows increased warming during FMA when compared to the corresponding annual trends. There is an exception, however: ERSST shows a very small cooling trend in the GOM from both 1887-2012 and 1870-2023, though this cooling trend is so small, it is nearly zero. The longer record (1870-2023) shows an enhanced warming trend of 0.0038 °C per year in the GOM, compared with the shorter record (1887-2012) at 0.0029 °C per year. However, ERSST shows less cooling in the GOM from 1870-2023 than 1887-2012 and a trend decrease by 0.0013 °C in 1870-2023 than the shorter record in the Caribbean. In FMA, CESM data show warming trends that exceed HadISST and ERSST trends, as opposed to smaller trends found in Table 3.1. The CESM trends in FMA are surpassed only by the coral reconstructions, which are an order of magnitude larger than the other data trends.

To compare the coral trends by location, a composite of FMA SSTA trends for HadISST (Figure 3.2a) and ERSST (Figure 3.2b) with the trends of each coral location is shown. The Cuba, Flower Garden Banks, Tobago, Guadeloupe, and Little Cayman trends (0.016, 0.0165, 0.0274, 0.0165, and 0.0217 °C per year, respectively) are warmer than the surrounding HadISST and ERSST trends. Dry Tortugas (0.0002 °C per year), however, is similar to the surrounding trends, particularly in ERSST (Figure

GOM Annual

Coral	*Dry Tortugas*	*Cuba*	*Flower Garden Banks*	*Average of Trends*	*Average of Records 1887-2012*
	7.155 * 10^-5	0.0013	0.0014	0.0009	0.0008
Gridded Data	*HadISST 1870-2023*	*ERSST 1870-2023*	*HadISST 1887-2012*	*ERSST 1887-2012*	
	0.0033	0.0015	0.0029	0.0030	
CESM	*Average 1887-2012*				
	0.00049				

CBN Annual

Coral	*Tobago*	*Guadeloupe*	*Little Cayman*	*Average of Trends*	*Average of Records 1887-2012*
	0.0020	0.0011	0.0019	0.0017	0.0013
Gridded Data	*HadISST 1870-2023*	*ERSST 1870-2023*	*HadISST 1887-2012*	*ERSST 1887-2012*	
	0.0050	0.0048	0.0051	0.0059	
CESM	*Average 1887-2012*				
	0.00056				

Table 3.1: Annual SSTA trends in the GOM and Caribbean separated by data used and region. Boxes indicates the years used to compute the trends were 1887-2012. Years across each coral site were inconsistent. As such, the trends per coral site were calculated using the record length available for that particular coral. Units: °C per year. SSTA trends from each record were all found to be significant, except Dry Tortugas FMA, using linear regression and t-test, though the resulting p-values could be the result of the correlation between years and SSTAs being significant. Significance and trends were then calculated using a polyfit, though the significance of the resulting slopes and p-vales were the same.

GOM FMA

Coral	*Dry Tortugas*	*Cuba*	*Flower Garden Banks*	*Average of Trends*	*Average of Records 1887-2012*
	0.00020	0.016	0.0165	0.0109	0.0109
Gridded Data	*HadISST 1870-2023*	*ERSST 1870-2023*	*HadISST 1887-2012*	*ERSST 1887-2012*	
	0.0038	-0.0006	0.0029	-0.00020	
CESM	*Average 1887-2012*				
	0.0039				

CBN FMA

Coral	*Tobago*	*Guadeloupe*	*Little Cayman*	*Average of Trends*	*Average of Records 1887-2012*
	0.0274	0.017	0.0217	0.022	0.016
Gridded Data	*HadISST 1870-2023*	*ERSST 1870-2023*	*HadISST 1887-2012*	*ERSST 1887-2012*	
	0.0051	0.0051	0.0054	0.0065	
CESM	*Average 1887-2012*				
	0.0061				

Table 3.2: Same as Table 3.1, for the spring months FMA.

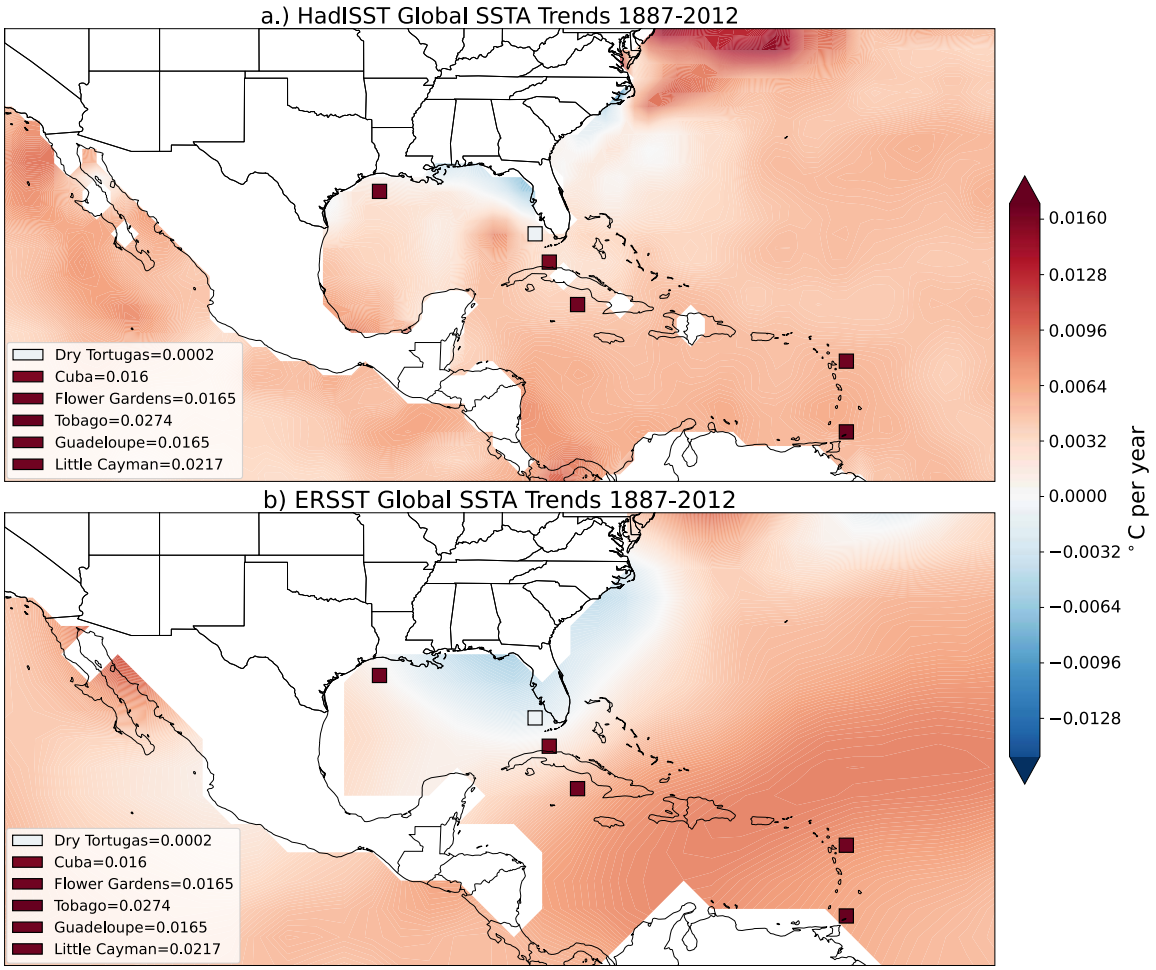


Figure 3.2: Composite of SSTA trends by grid point in the IAS during FMA using (a) HadISST and (b) ERSST. Squares correspond to the FMA SSTA trends at each coral location. Trends are in ℃ per year.

3.2b). A more expansive region of lower trends, in some cases cooling trends around -0.005 ℃ per year, surrounds Florida's coasts and extends up the northeast coast and west into the GOM in both HadISST and ERSST, with a larger extent in ERSST. This perspective offers insight into the spatial distribution of trends as the average negative ERSST trend in the GOM during FMA (-0.0002 ℃ per year) can be more easily explained. For HadISST, the cooler trends in the GOM do not extend as far away from the coastlines, resulting in a warmer average trend than ERSST. These composites

also show enhanced warming in the Caribbean when compared to the GOM for both, HadISST and ERSST.

3.1.2 GOM and Caribbean Power Spectra

Trends provide information regarding the variability of SSTAs in each region. To determine potential causes, standardized SSTAs were used to conduct power spectra analyses, evaluating the common and unique periodicities between regions. These analyses were repeated for each dataset and across the spring (FMA), summer (June, July, August), and winter (November, December, January) months to determine how the significant periods vary with season. Significant periods were calculated by comparing periods to the null hypothesis spectra using a red-noise process as well as chi-squared significant tests at 90% and 95% confidence intervals. The squared coherence and phase relationship at significant periods were also calculated.

In FMA, HadISST, ERSST, and coral reconstructions each indicate a weakly negative correlation between GOM and Caribbean detrended SSTAs (Figures 3.3, 3.4). Though the correlations are weak (-0.29, -0.26, and -0.07, respectively), they were significant with p-values below 0.05 for HadISST and ERRST, and not significant for coral data. This negative correlation was expected during the springtime when the dipole occurs, when the largest difference between the Caribbean and GOM occurs and supports findings in previous studies (Muñoz et al., 2010).

HadISST power spectrum of FMA showed no significant periods in the Caribbean, and one significant period at 4.9 years in the GOM, within ENSO periodicity (Figure 3.3). Similarly, a significant period at 4.9 years is shown in the GOM using ERSST (Appendix A.1). However, ERSST also indicated a significant period at 42 years in the Caribbean. While some differences are present between HadISST and ERSST, there is mostly agreement in terms of significant periods, significant squared coherence and

phases differences. As such, ERSST power spectra figures can be found in the appendix. However, the coral reconstruction power spectra deviated from HadISST and ERSST with significant periods at 28 and 21 years in the GOM, possibly indicating decadal variability (such as PDO), and 7 years in the Caribbean, indicative of ENSO (Figure 3.4).

Coherence squared is analogous to correlation in the frequency domain and is useful in determining the relationship between two time series, in this case GOM and Caribbean SSTAs. HadISST and ERSST demonstrated similar coherence squared, significant around 15, 13, and 4.5 years where a fraction of variance of CBN SSTAs can be ascertained from GOM SSTAs (Figure 3.3. Phase difference between the GOM and Caribbean is shown when squared coherence is significant (Figure 3.3). There is no significant period in which the GOM and the Caribbean SSTAs are in phase with one another. In fact, the phase differences at each significant peak are negative, indicating the GOM signal is leading the CBN in the springtime. This is also supported by the coral record as two out of the three significant phase differences in this record during FMA are negative and occur around a period of 13 years (angular frequency of 0.5). In the ERSST and coral records, each has a single positive phase difference at periods of 5.7 and 8 years (angular frequencies of 1.2 and 0.75), respectively. In these instances, the GOM lags behind the Caribbean, differing from HadISST.

In JJA, there is a significant, stronger positive correlation between the GOM and the Caribbean for HadISST and ERSST (0.5 and 0.64 respectively), and a very weak positive correlation when using coral data (0.08), though this correlation is not significant. Muñoz et al. (2010) similarly found positive correlation between SSTAs in each region during summer months. The examination of months outside of spring provides information on how the GOM and Caribbean are co-varying. Significant periods for HadISST include 9.3 years in the GOM, and 16.8 years in the Caribbean (Figure 3.5).

For ERSST, the significant periods were found to be 4.2 and 4.4 years in the GOM and no significant periods in the Caribbean (not shown). Significant periods in coral records include 40 and 26.7 years in the GOM, and 40 and 4.2 years in the Caribbean (3.6). Though the significant periods in JJA differ from FMA, there appears to still be common periodicity with ENSO, particularly in HadISST and ERSST as well as in the Caribbean in the coral records. In particular, HadISST found a significant period in the Caribbean in JJA and not in FMA. ERSST, however, did not find a significant period in the Caribbean in JJA but did in FMA. Unlike FMA, coral data found longer periods in GOM, and a multi-decadal period in the Caribbean in JJA. Once again, the coral records denoted significant signals at multi-decadal periodicities. In constrast to FMA, in JJA all three data types indicated majority positive phase differences, or the GOM SSTAs lag behind the Caribbean, as indicated by phase angles above zero. In each, HadISST, ERSST, and coral records, no phase difference was apparent between the GOM and Caribbean at periods close to 4 years (angular frequency of 1.6) (Figures 3.5d, 3.6d, and ERSST can be found in the Appendix). However, HadISST and ERSST have an additional instance of near-zero phase difference at periods near 21 years (angular frequency of 0.3).

During winter months, there was more squared coherence, and phase difference variation between records. As such, all three power spectra were included in this section. Correlations between the GOM and the Caribbean were found to be very weakly positive using HadISST and ERSST, and very weakly negative using coral records (0.008, 0.14, -0.13 respectively). Each correlation was found to be not significant. The coral correlation, however, most closely aligns with Muñoz et al. (2010) that found a correlation of -0.16 in NDJ. Significant periods at 21 years in the GOM and 7.6 and 42 years in the Caribbean were found using HadISST while 4.7 years in the GOM and 42 and 7.6 years in the Caribbean were found using ERSST (Figures 3.7, 3.8. Coral records

showed significant periods at 28 years in the GOM and 7.6 years in the Caribbean (Figure 3.9). Similar to previously discussed seasons, there are periodicties that fall within ENSO periodicity as well as multi-decadal periodicities. It is important to note that during NDJ, there is a common periodicity of 7.6 years in the Caribbean across all records. The coherence squared is inconsistent across HadISST, ERSST, and coral records. Additionally, in HadISST, in all cases of significant squared coherence, phase differences are negative, so the GOM is leading the Caribbean. ERSST shows a majority of negative phases with one positive and two near-zero. Though both, HadISST and ERSST indicate negative phase difference between periods 16-31 and 5-6 years (angular frequencies between 0.4-0.2 and 1.2-1). The coral record phases between the GOM and the Caribbean largely differ from ERSST and HadISST with positive phases between similar period ranges. It is important to examine why the winter months show increased variation in phases between the GOM and the Caribbean than spring and summer months while also having a common periodicity across all records.

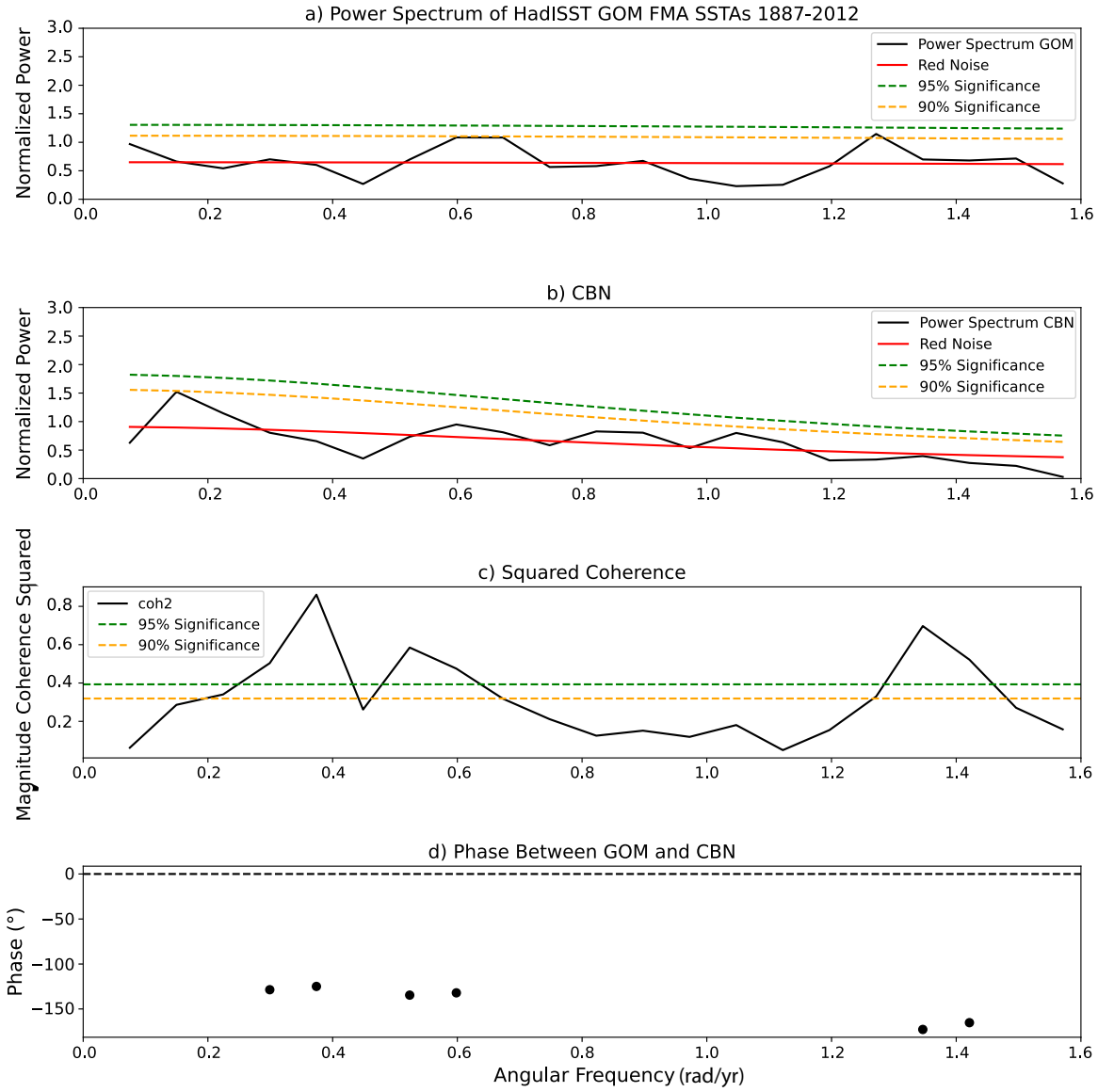


Figure 3.3: Spectral analysis of area-averaged, detrended, standardized SSTAs using HadISST for the (a) GOM and (b) Caribbean during FMA from 1887-2012. In panels a-b, the SSTAs (black-solid), red noise (red-solid), 95% (green-dashed) and 90% (orange) significance are shown. (c) Coherence squared between the GOM and Caribbean time series shown with 95% and 90% significance. (d) Phase relationship between the time series, only shown when coherence squared is significant at 95%. Phase difference is zero at the dashed line.

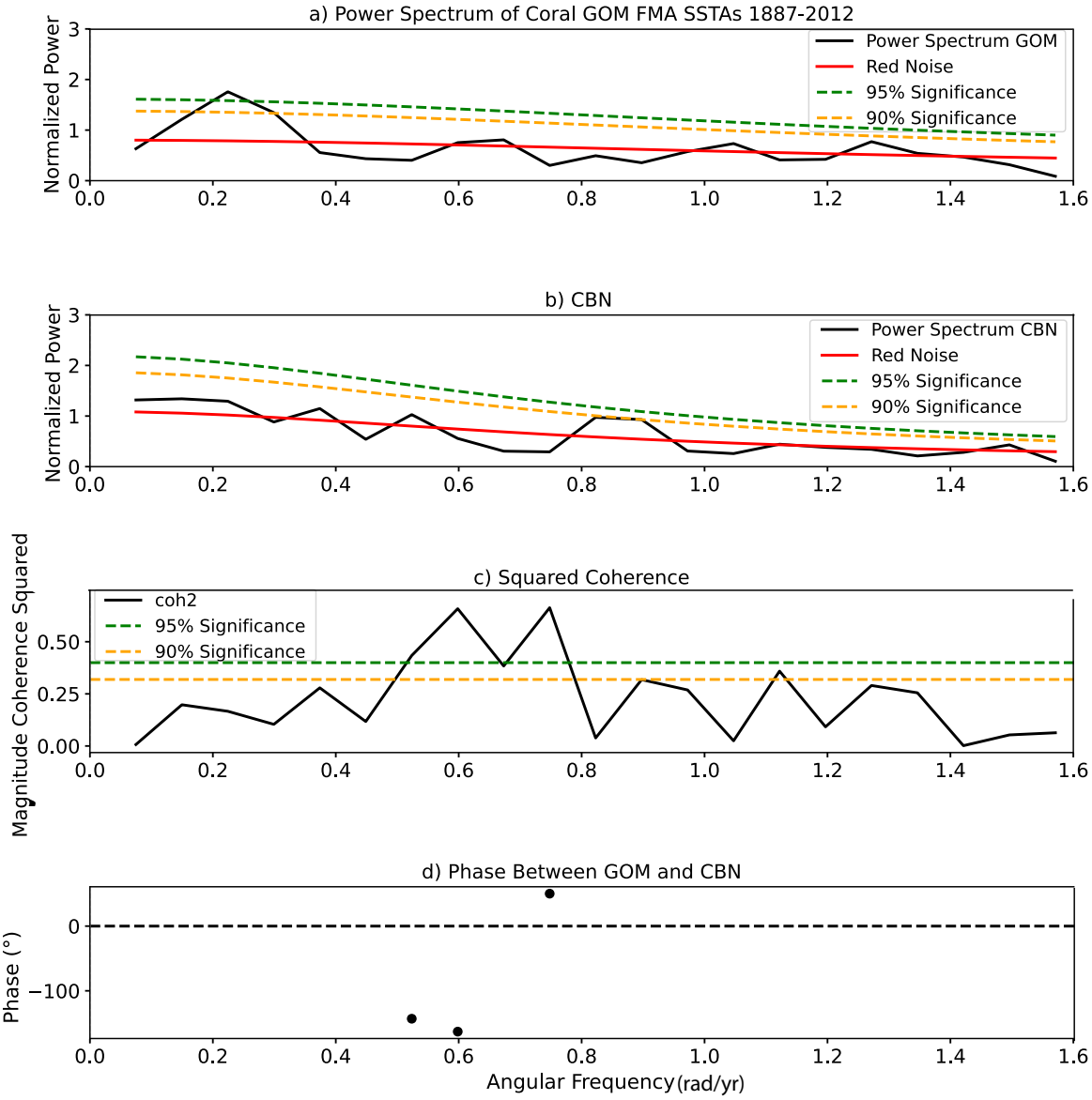


Figure 3.4: Same as Figure 3.2 except with coral reconstructions.

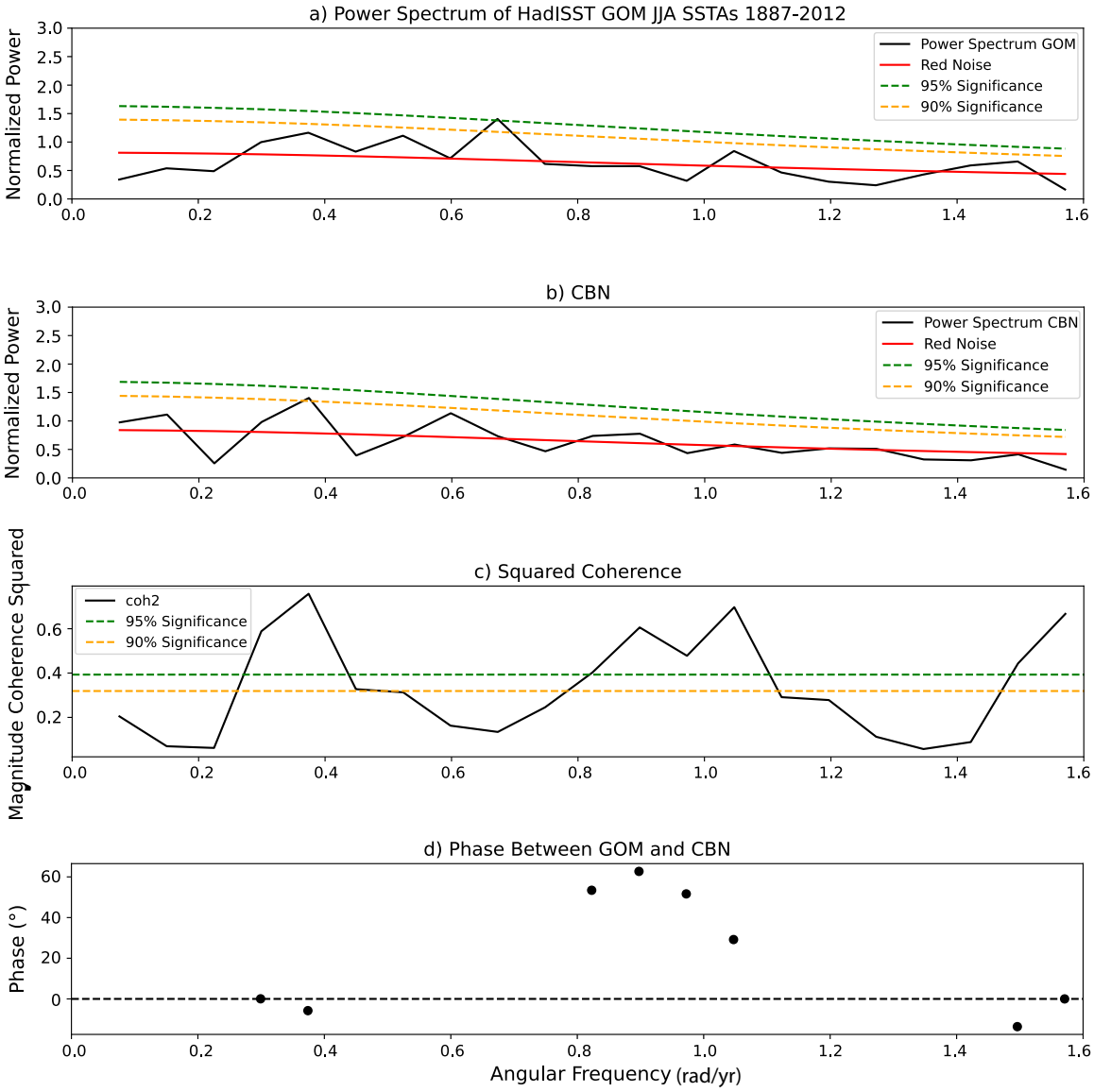


Figure 3.5: Spectral analysis of area-averaged, detrended, standardized SSTAs using HadISST for the (a) GOM and (b) Caribbean during JJA from 1887-2012. In panels a-b, the SSTAs (black-solid), red noise (red-solid), 95% (green-dashed) and 90% (orange) significance are shown. (c) Coherence squared between the GOM and Caribbean time series shown with 95% and 90% significance. (d) Phase relationship between the time series, only shown when coherence squared is significant at 95%. Phase difference is zero at the dashed line.

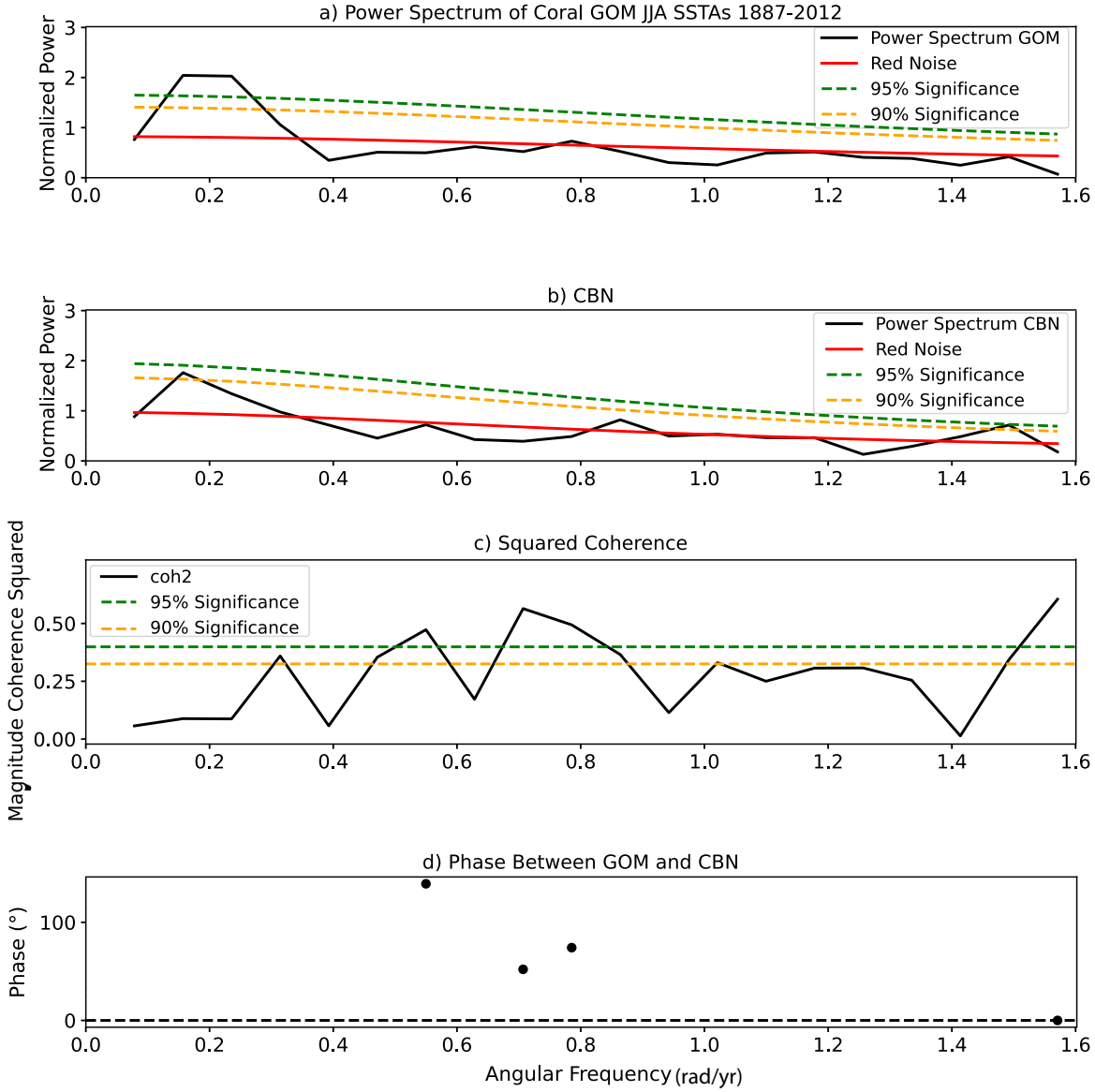


Figure 3.6: Same as Figure 3.4 except with coral reconstructions.

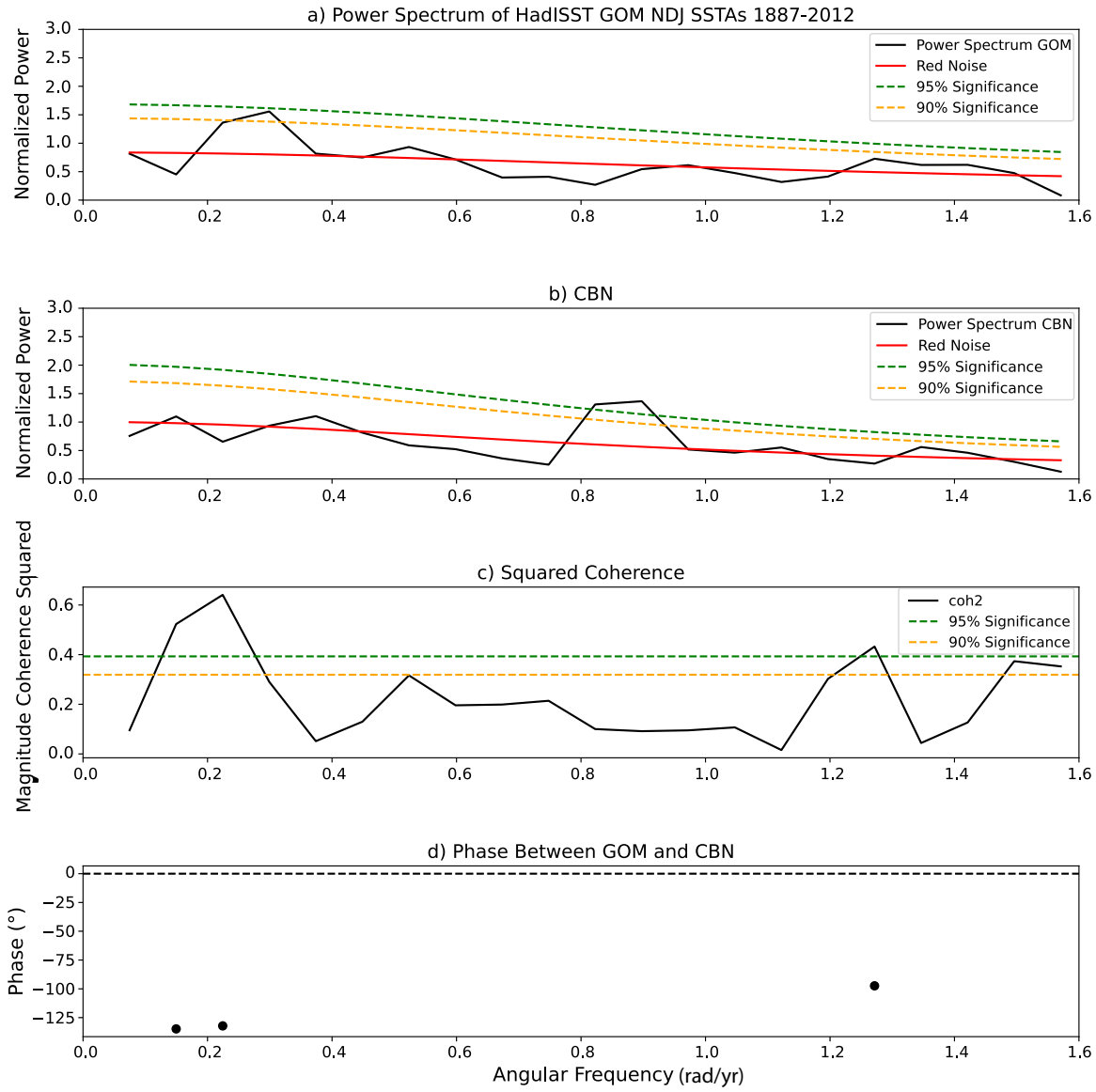


Figure 3.7: Spectral analysis of area-averaged, detrended, standardized SSTAs using HadISST for the (a) GOM and (b) Caribbean during NDJ from 1887-2012. In panels a-b, the SSTAs (black-solid), red noise (red-solid), 95% (green-dashed) and 90% (orange) significance are shown. (c) Coherence squared between the GOM and Caribbean time series shown with 95% and 90% significance. (d) Phase relationship between the time series, only shown when coherence squared is significant at 95%. Phase difference is zero at the dashed line.

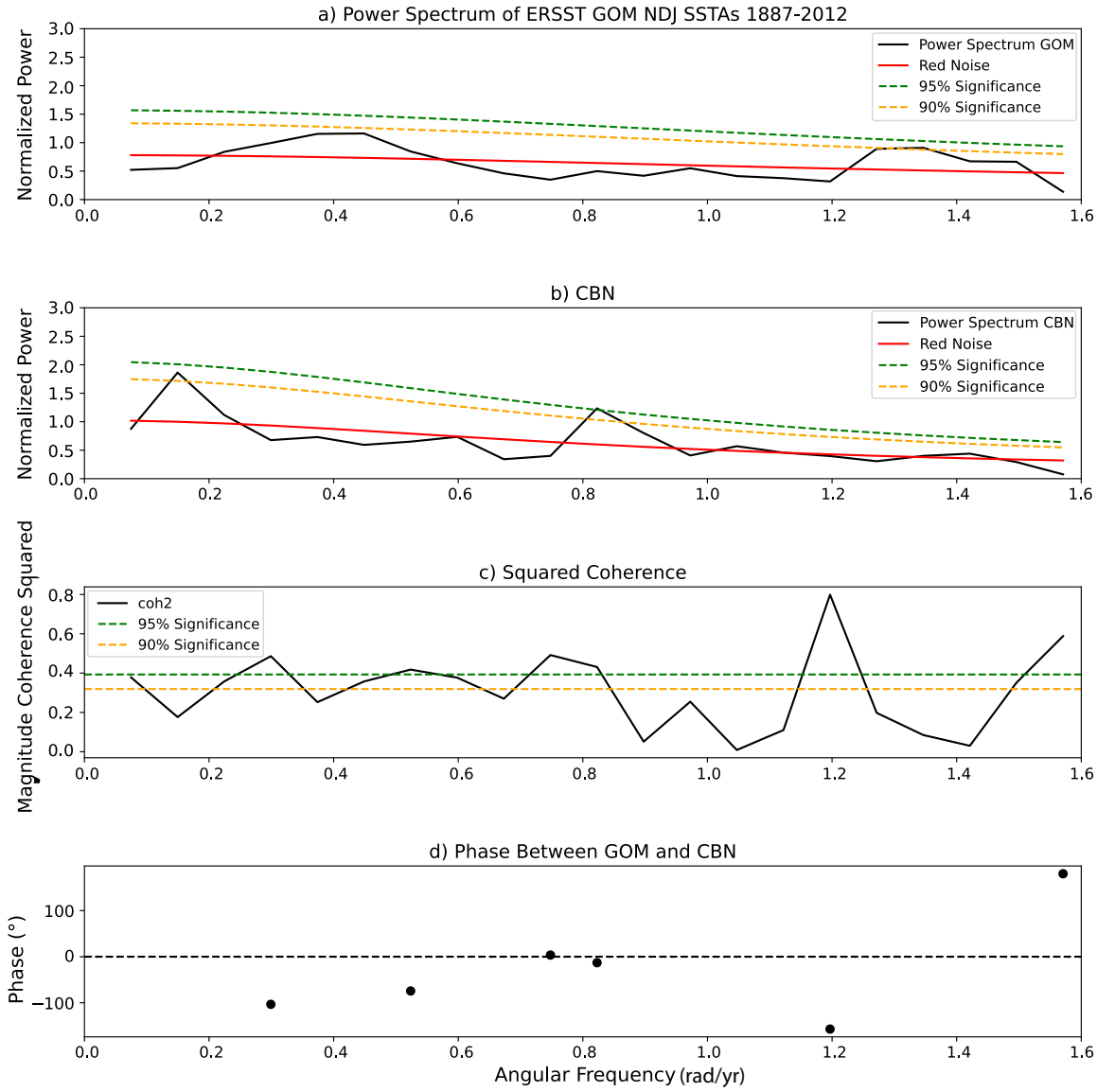


Figure 3.8: Same as Figure 3.6 except with ERSST.

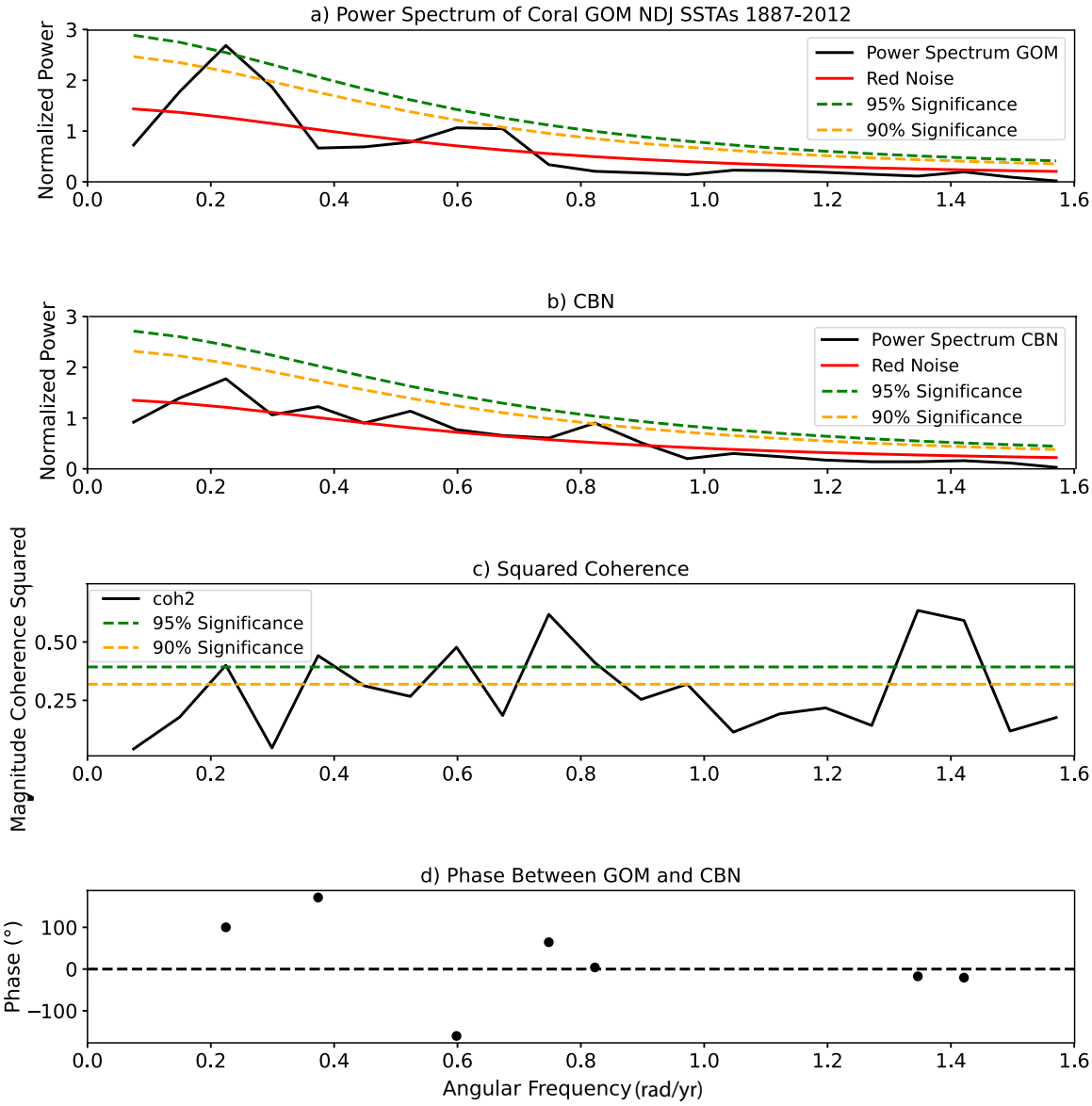


Figure 3.9: Same as Figure 3.6 except with coral reconstructions.

3.2 Springtime Sea Surface Temperature Anomaly Dipole

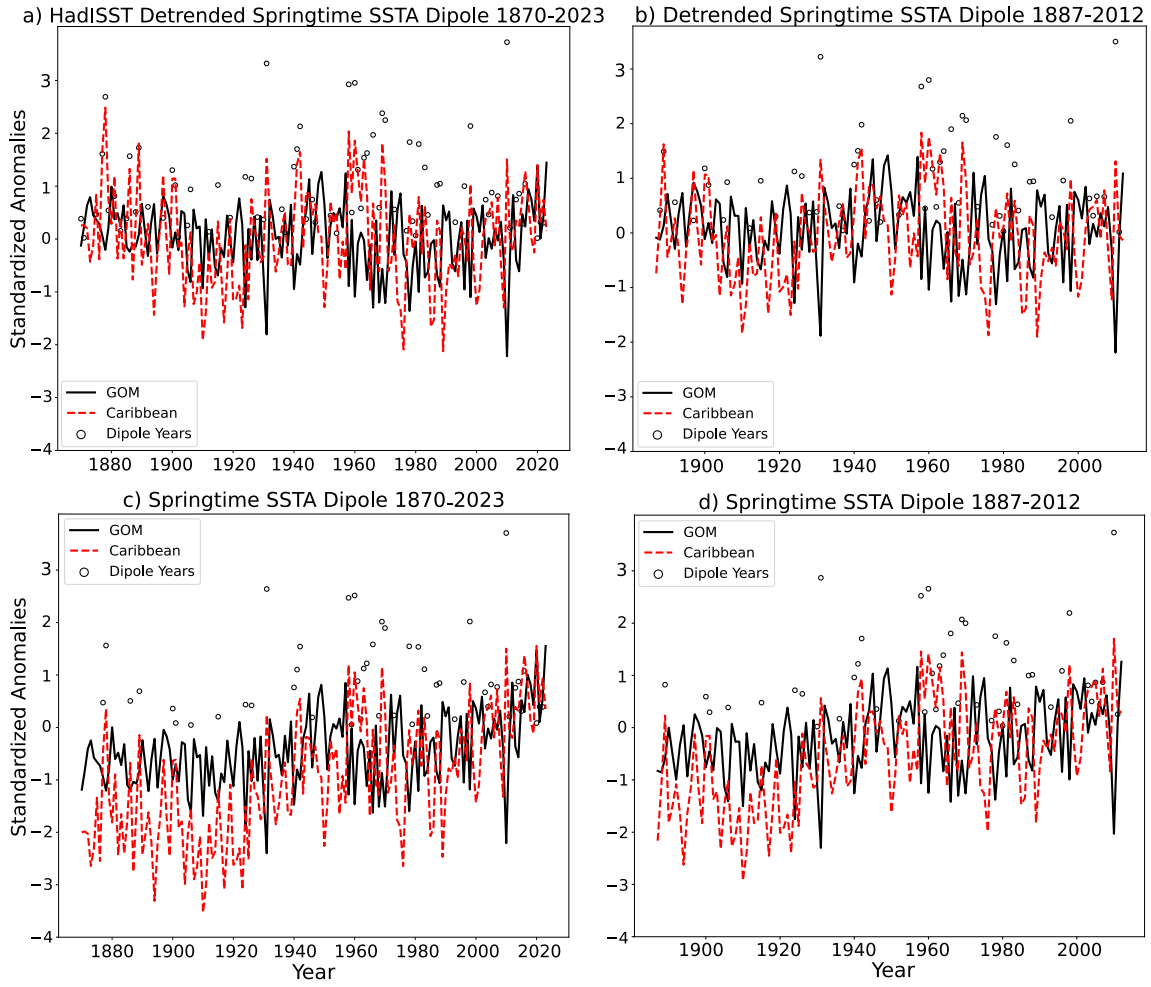


Figure 3.10: Detrended standardized FMA SSTAs and dipole years using HadISST from (a) 1870-2023 and (b) 1887-2012. Standardized SSTAs and dipole years from (c) 1870-2023 and (d) 1887-2012. In all panels, GOM (black-solid), Caribbean (red-dashed), and dipole years (circles) are shown.

With a better understanding of the variability of SSTAs in the IAS, the SSAD and how it has changed over time with and without the linear warming trend was

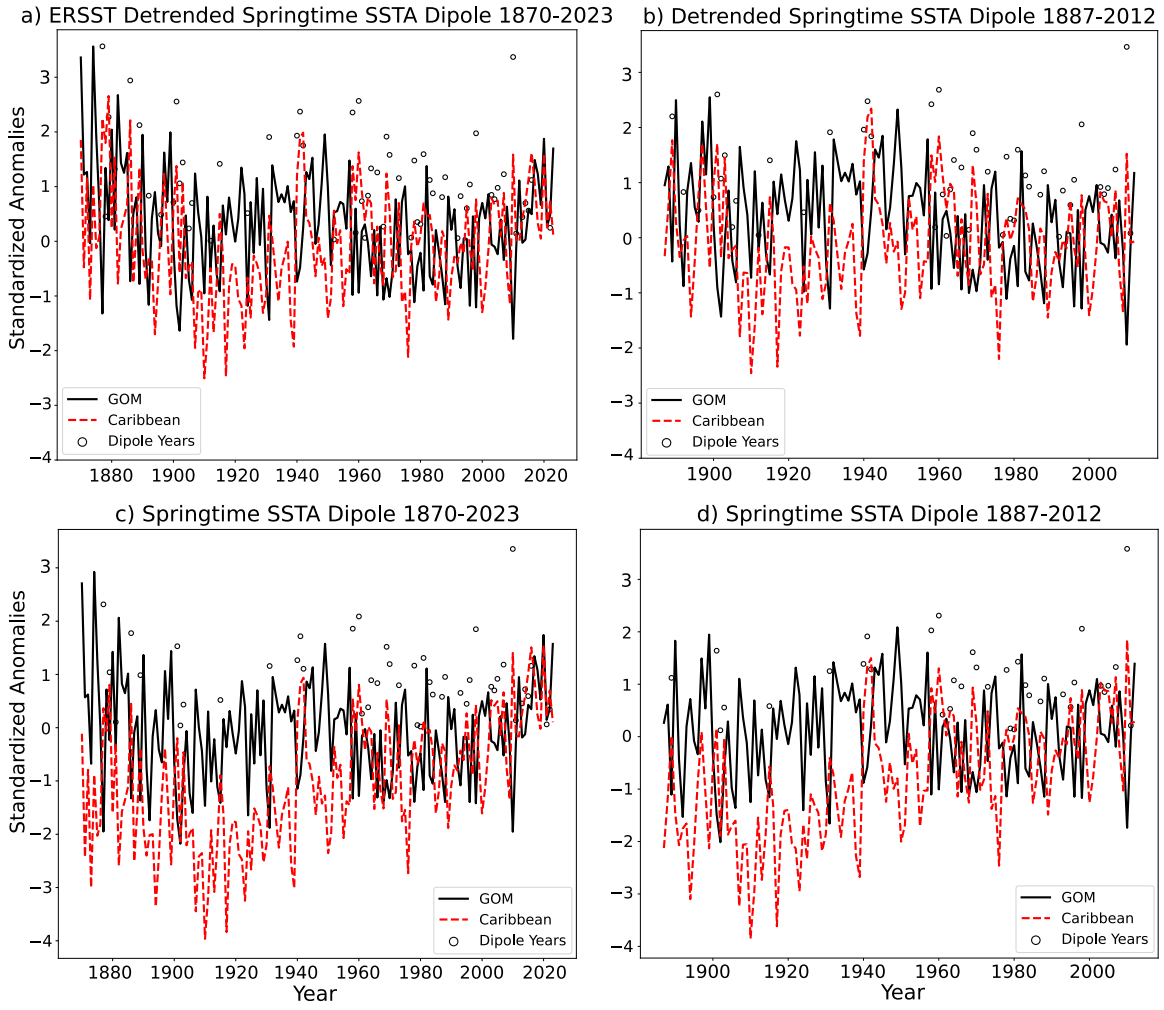


Figure 3.11: Same as Figure 3.9 except with ERSST.

examined. Figure 3.10 shows time series of the IAS detrended SSTAs (Figure 3.10a, b) and the SSTAs not detrended (3.10c, d). A longer record length, 1870-2023 was included to examine the role of the long-term trends shown in Section 3.1. Circles indicate a year in which a dipole was present. Panels c and d in Figure 3.10, include the warming trend. Earlier in the record, the Caribbean was anomalously cooler than the GOM, inhibiting frequent dipole formation prior to 1930. As the Caribbean warmed faster than the GOM, dipole occurrence increased. Detrending the data removed the anomalously cool SSTAs in the Caribbean earlier in the record, lending to more dipole

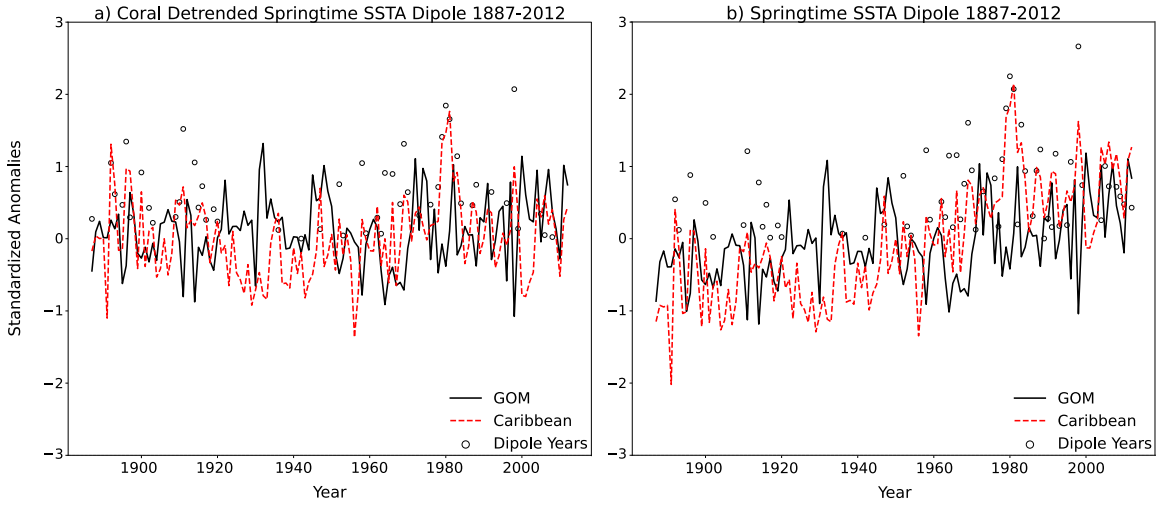


Figure 3.12: Same as Figure 3.9 except with coral reconstructions and only 1887-2012.

occurrences without the trend than with it. Similar to HadISST, ERSST not detrended SSTAs were cooler prior to 1940 and warmed at a faster rate than the GOM (3.11c, d). However, the GOM SSTAs in ERSST were warmer than the GOM SSTAs in HadISST, particularly during the first half of the record. Similarly, using ERSST, more dipole years occurred without the warming trend (3.11). The magnitudes of the plotted dipole years indicate the degree of difference between the anomalies and likely a large magnitude indicates both regions particularly anomalous. For instance, 1931 had a large dipole magnitude. In this year, the standardized anomaly in FMA in the GOM was around -1.8 (anomalously cool) and 1.5 (anomalously warm) in the Caribbean (Figure 3.10a, b). In other words, the anomalies were opposite and nearly symmetric. However, the 1990s were dominated by non-dipole years, with several decades of more frequent dipole years preceding as well as increased dipole occurrences from 2000-2012 in the 1887-2012 record for both detrended and non-detrended data. Figure 3.10a, and c include 1870-2023 and show similar results to 1887-2012 except include an intense dipole prior to 1880 and the years 2013-2023 where fewer dipoles are present. There was more variation between SSTAs in the GOM and the Caribbean found in ERSST

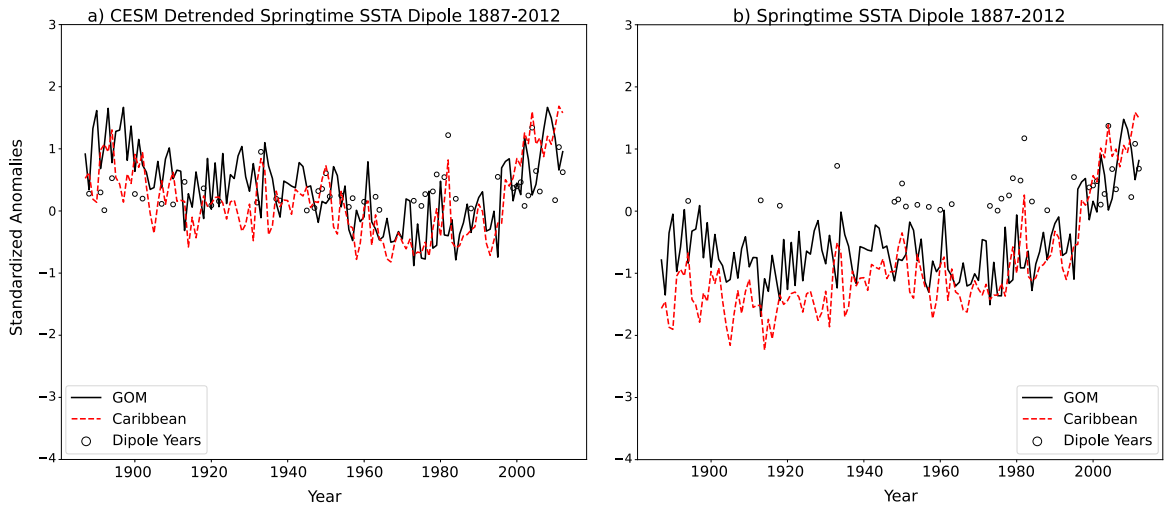


Figure 3.13: FMA SSTAs and dipole years using CESM2 LENS2 ensemble members 1-10 from 1887-2012 (a) detrended and (b) not detrended. SSTAs found for each ensemble member, then averaged together before finding the dipole index. Figure is used to compare average number of dipoles from 1887-2012 with other records, not to compare specific years of dipole occurrences. In all panels, GOM (black-solid), Caribbean (red-dashed), and dipole years (circles) are shown.

than HadISST: in the GOM, detrended SSTAs range from -1.75 to over 3.0 and in the Caribbean from -2.5 to 2.5 (3.11a, b).

The range of SSTAs in the coral record (-1 to 1.5 in the GOM and -1.2 to 1.75 in the Caribbean) resembles HadISST over ERSST, though dipole years match neither observation record (Figure 3.12). In contrast with HadISST and ERSST, more dipoles occurred in the SSTA time series that was not detrended (Figure 3.12). This is likely due, in part to the warmer Caribbean SSTAs in the first half of the record, allowing for more dipole occurrences prior to the 1940s. CESM ensemble mean resulted in the narrowest range of SSTAs in each region from 1887-2012, likely due to the smoothing of natural variability (Figure 3.13). The SSTAs in the GOM were anomalously warm throughout most of the record except from around 1950-1990, with more dipole occurrences during this 40 year period than the previous 40 years (Figure 3.13a). Smaller differences between CESM SSTAs in the GOM and the Caribbean led to decreased

dipole magnitude compared to the other records. The detrended SSTAs were warmer in both regions than in other records, however, CESM is in agreement with the other records in that the Caribbean warming trend increased at a faster rate than the GOM, resulting in less dipole occurrences prior to 1940 and less dipoles in the not detrended SSTAs than the detrended counterpart. Generally, all four records exhibited enhanced warming in the Caribbean compared to the GOM, supporting the results found in Table 3.2. For HadISST, ERSST, and CESM this warming inhibited the formation of dipoles during the first half of the records. The warmer Caribbean coral SSTAs allowed for dipole formation during the first decades of the record leading to more dipole occurrences in the non-detrended SSTA time series than the detrended, opposite of HadISST, ERSST, and CESM.

Tables 3.3 and 3.4 provide another form of dipole comparison across all records used in this study. Dipoles per decade were calculated between each coral site in the GOM and each site in the Caribbean, across the shared record length (Table 3.3). These were then averaged to around 3.8 dipole years per decade. Each of the coral site pairings resulted in a dipoles per decade range between 4 and 5, with GOM pairings with Tobago in the Caribbean being the exception with less than 4 per decade. Dipole calculation executed after interpolation and averaging SSTAs in the GOM and also the Caribbean resulted in an average of 4.08 dipoles per decade for standardized, detrended SSTAs and 5 dipoles per decade for not detrended, standardized SSTAs (Table 3.4). This result is inline with HadISST, ERSST, and CESM dipoles per decade with 4.67, 4, and 4.08 dipoles per decade, respectively for standardized, detrended SSTAs. Though observations and CESM are in agreement with reduced dipole occurrences when the warming trend is not removed, coral SSTAs indicate increased dipole occurrences with the trend present. HadISST has significantly more dipole occurrences than ERSST

from 1870-2023, however, is closer to the other records when only considering 1887-2012. Coral data and the average of CESM members both indicate 49 total dipoles from 1887-2012 or 4.08 dipole per decade when using standardized, detrended SSTAs. Dipoles per decade per CESM ensemble member are within the range 3.8-5.2. Without removing the warming trends, these two records differ significantly with 5 dipoles per decade in the coral record and 2.75 according to CESM.

Composites of SSTAs were used to examine the SSAD spatial pattern and how it differs between datasets. SSADs are categorized as cooler SSTAs in the GOM and warmer SSTAs in the Caribbean. This setup can be seen in Figure 3.14 where a composite of dipole years, non-dipole years, and the composite difference for FMA is shown. As expected, during dipole years found using HadISST, cooler anomalies below 0°C in the GOM, with a minimum along the coast of Texas, extend into the North Atlantic, and warmer anomalies in the Caribbean extend into the Atlantic, maximizing in the southern and eastern Caribbean. During dipole years, the Pacific is also anomalously warm. During non-dipole years, or years in which a cool GOM, warm Caribbean dipole was not found, the opposite pattern is found: warmer SSTAs

Coral Dipoles Per Decade	*Dry Tortugas*	*Cuba*	*Flower Garden Banks*	*GOM Average*
Tobago	2.5	3	1.5	3.5
Guadeloupe	4.5	4.9	4.9	4.2
Little Cayman	4.2	4.8	4.7	4.5
CBN Average	3.8	4.8	4.8	3.8

Table 3.3: Dipole occurrences per decade per coral location. Dipole index is calculated with each pairing combination of GOM and Caribbean coral sites. Common years were used for each pairing, in some cases only a few decades were available for the dipole calculation.

Dipoles by Data Type

Corals	*Average SD DET*	*Average SD*		
Total 1887-2012	49	60		
Per decade	4.08	5		
Observations	*HadISST SD DET*	*ERSST SD DET*	*HadISST SD*	*ERSST SD*
Total 1870-2023	74	59	50	46
Per decade	4.93	3.93	3.33	3.07
Total 1887-2012	56	48	48	36
Per decade	4.67	4	4	3
CESM	*Average SD DET*	*Average SD*		
Total 1887-2012	56	33		
Per decade	4.68	2.75		

Table 3.4: Dipole occurrence totals and per decade per data type. "SD" refers to standardized SSTAs and "SD DET" refers to standardized detrended SSTAs. Coral dipole calculation in this table was performed after interpolating and averaging coral records in each region, resulting in a different per decade value than Table 3.3. CESM dipoles found after averaging the first ten model members SSTAs.

in the GOM and North Atlantic, and cooler SSTAs in the Caribbean extending into the Atlantic with a cooler Pacific as well, considered a "reverse dipole" or a non-dipole. The composite difference and significance were unsurprising as warmer SSTAs subtracted from cooler anomalies in the GOM results in even cooler SSTAs and vice versa for the Caribbean, with differences below -1°C in the western GOM and exceeding 1.5°C in the eastern Caribbean. Repeating the composites with ERSST, the results were similar with a cool GOM extending into the North Atlantic, and a warm Caribbean, Atlantic, and Pacific during dipole years (Figure 3.15. During non-dipole years, ERSST shows enhanced warm SSTAs in the GOM compared to HadISST with values exceeding 1°C across much of the region. Given the repetitive nature of the results, the same composites for an extended record length of 1870-2023 using HadISST and ERSST can be found in the Appendix.

Composites examining whether SSADs are associated with SSTA patterns in proceeding seasons, hurricane season (June-November), boreal summer (JJA), and winter months (NDJ), are shown in Figures 3.16 and 3.17. This analysis is important to fully understand the scope of the potentially persisting impacts of SSADs. The FMA SSAD pattern persists as SSTAs indicate a larger region of warmer temperatures, primarily in the Caribbean (SSTAs between 0.5 and 1), and still slightly cooler temperatures, though reduced in extent, in the GOM (below 0.5) during June-November in HadISST and ERSST, though the cooler GOM is more apparent in ERSST (Figure 3.16a, Figure 3.17a). However, during non-dipole years, both the GOM and the Caribbean are anomalously cool with pockets of slightly warmer SSTAs in the GOM along the coast of Mexico as well as in the Pacific along the west coast of Mexico. JJA is part of the hurricane season thus has a similar spatial springtime dipole pattern (Figure 3.16b, Figure 3.17b). Non-dipole years patterns are again similar to June-November, with even cooler anomalies in the Caribbean and parts of the GOM in both HadISST and

ERSST. NDJ composites are most similar to FMA during both dipole and non-dipole years in the GOM and the Caribbean (Figure 3.16c, Figure 3.17c). However, the Pacific is cooler during dipole years and warmer during non-dipole years in NDJ for both HadISST and ERSST, which is the opposite in FMA. November was found to be a month with large difference between SSTs in the GOM and the Caribbean which could explain the cool-warm dipole setup in the IAS during NDJ (Figure 2.5c, d).

3.2.1 Atlantic Warm Pool

An important summertime phenomena is the AWP, a region in the North Atlantic with SSTs exceeding 28.5 °C. The largest extent and greatest intensity of the AWP occurs in the summer, following a SSAD or a non-dipole. The previous section showed the spatial distribution of SSTAs during the summer that showed significant differences between dipoles and non-dipole years suggesting an impact on the size and intensity of the AWP. To examine this possible relationship between AWP size and intensity with SSADs, composites of SSTs in the IAS during dipole years and non-dipole years were compared. Figure 3.18 shows the extent of the AWP during the Atlantic hurricane season where the black contour indicates temperatures of 28.5℃ while the blue indicates temperatures of 29℃. First, HadISST qualitatively shows a larger extent of the AWP: the expansion of the 28.5℃ isotherm eastward in the Caribbean following dipoles than non-dipoles. Regions of increased intensity (29℃) are also enlarged following a dipole. ERSST has similar findings with increased extent and intensity following a dipole compared to a non-dipole. Though, ERSST does exhibit a smaller extent and reduced intensity when compared to HadISST. Given the repetitive nature of the results, the same composites for an extended record length of 1870-2023 using HadISST and ERSST can be found in the Appendix.

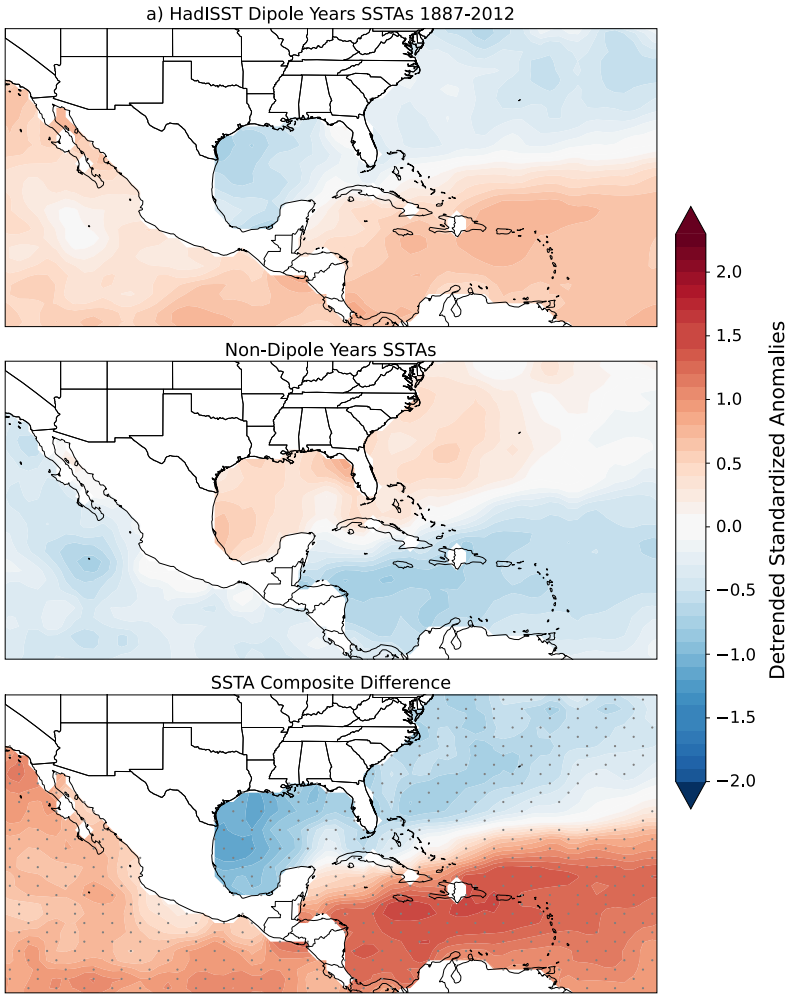


Figure 3.14: Composite of detrended standardized SSTAs in the IAS using HadISST from 1887-2012 during (top) dipole years, (middle) non-dipole years, and (bottom) composite difference with 99% confidence (gray dots) using a Monte Carlo test.

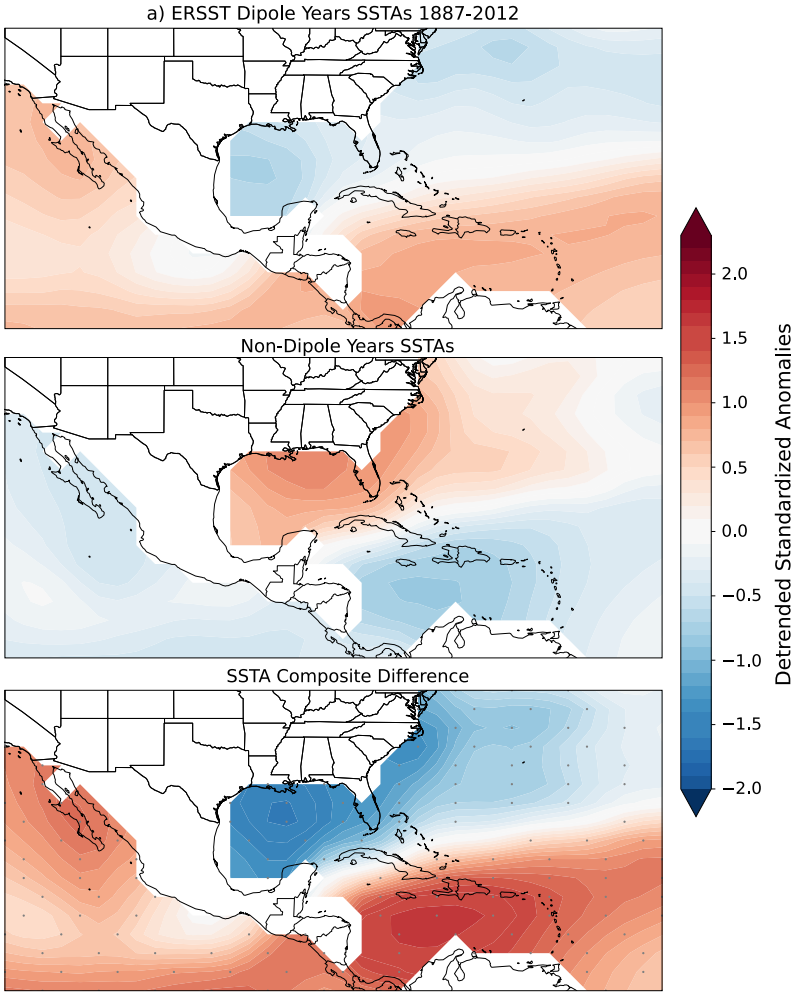


Figure 3.15: Same as Figure 3.13 except with ERSST.

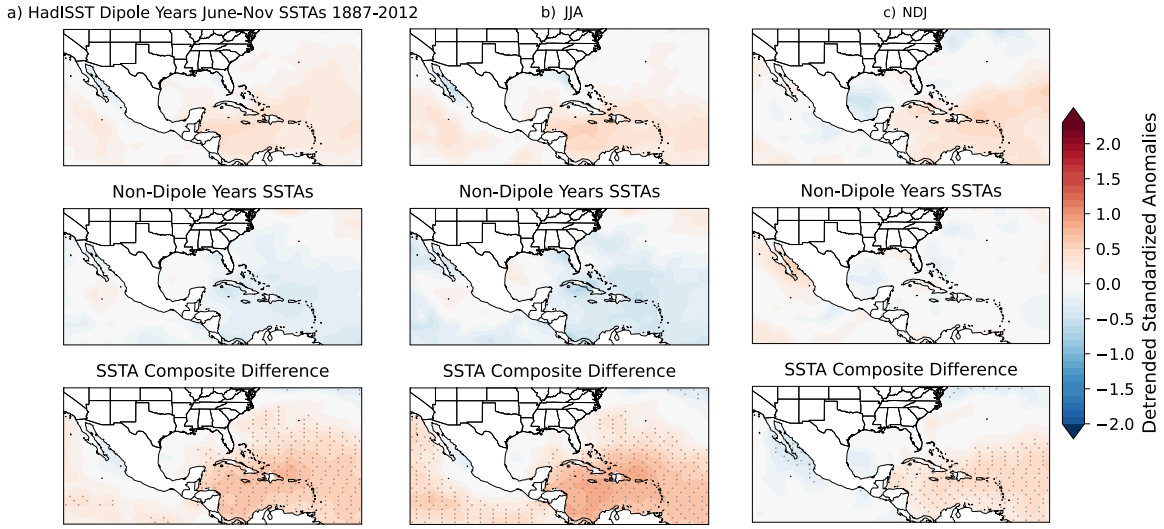


Figure 3.16: Composite of detrended standardized SSTAs in the IAS using HadISST from 1887-2012 during (a) June-November, (b) JJA, (c) NDJ for (top) dipole years, (middle) non-dipole years, and (bottom) composite difference with 99% confidence (gray dots) using a Monte Carlo test.

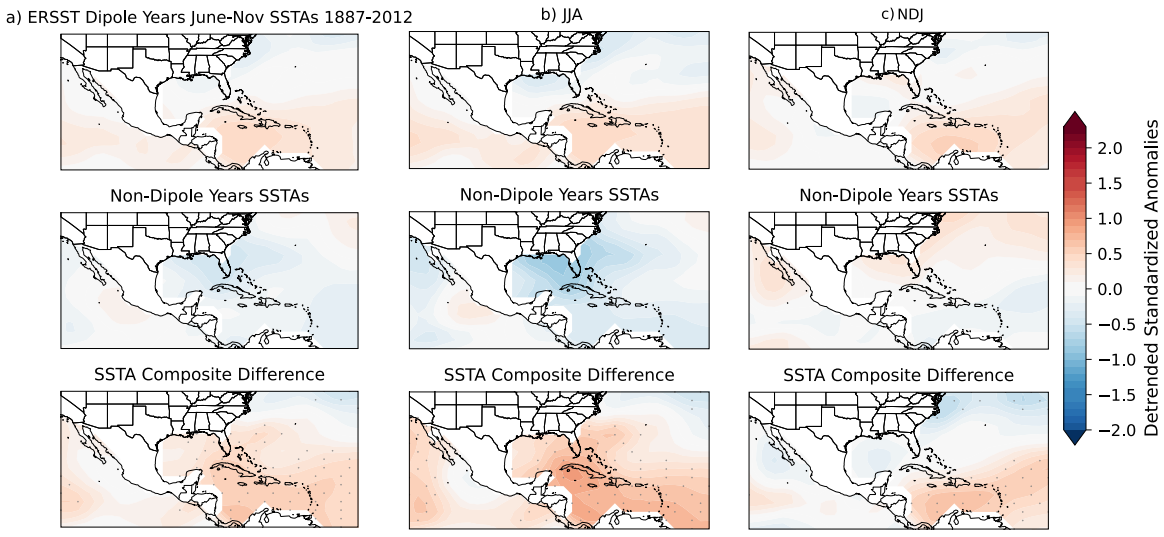


Figure 3.17: Same as Figure 3.15 except with ERSST.

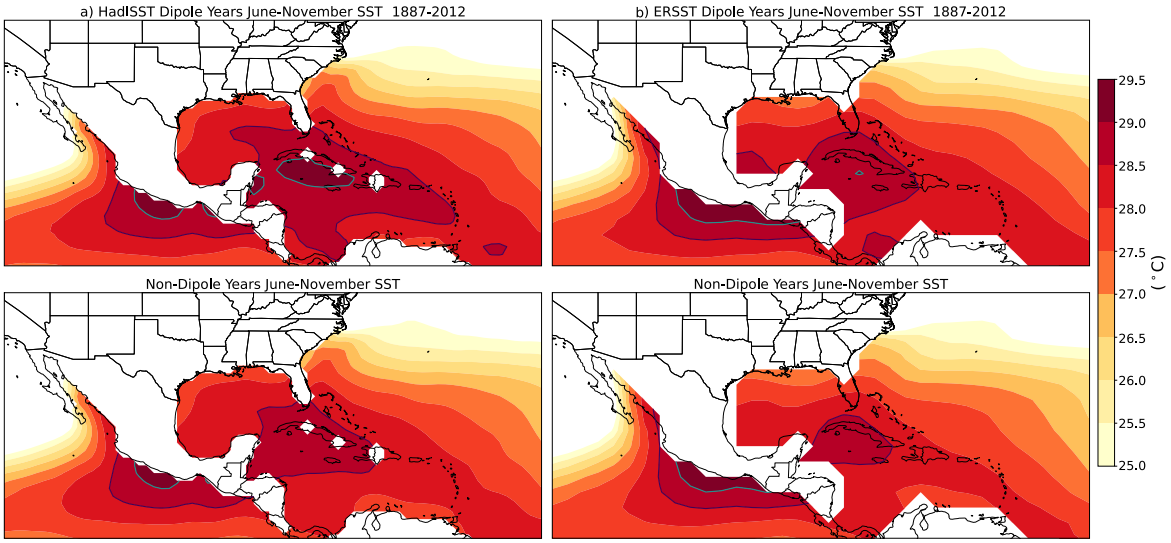


Figure 3.18: Composite of hurricane season-mean SSTs in the IAS from 1887-2012 using (a) HadISST and (b) ERSST during (top) dipole years, and (bottom) non-dipole years. Black contour at 28.5℃ and blue contour at 29.5℃.

Chapter 4

Discussion

4.1 Sea Surface Temperature Variability in the IAS

Given the importance of the IAS on regional climate across North America and parts of South America, an in depth comparison of SSTAs in the GOM and the Caribbean is necessary, particularly in the midst of a changing climate with the most recent two decades experiencing enhanced warming (Flannery et al., 2024; Manzello, 2015). Observations, coral proxies, and climate model output were used to compare the variability of SSTAs in each region over the past 125 and 150 years, increasing the record length from previous studies, and improving reliability of the conclusions drawn from this study (Muñoz et al., 2010). With a changing climate, it is expected the response of SSTs in the GOM and Caribbean differs. The Caribbean is warming faster than the GOM, average Caribbean SSTs are warmer than GOM SSTs, significant periodicities of SSTAs differ in each region, and each region is separately impacted by teleconnections.

The benefits of utilizing multiple data types is supported by the agreement across HadISST, ERSST, coral reconstructions, and CESM that trends in each region were congruous with previous studies as each record type indicated the Caribbean is warming at a faster rate than the GOM, both annually and during springtime. Anthropogenic climate change is projected to contribute to an increase in SSTs in the Atlantic leading to a reduction in the Atlantic Meridional Overturning Circulation (AMOC) (Liu et al., 2012). AMOC is a connection of large scale ocean circulations that act as a mechanism

that facilitates the distribution of heat poleward. The Loop Current is an important component of AMOC that directly impacts SSTs in the GOM. In particular, the Loop Current is responsible for bringing warm SSTs from the Caribbean into the GOM (Liu et al., 2012). Liu et al. (2012) studied AMOC weakening using high-resolution ocean circulation models and with a slow down of AMOC, there was a 20-25% decrease in volume transport by the Loop Current. This is particularly true in the Northern GOM as the extent of the Loop Current and the eddies that break off the Loop Current has decreased. This may have two possible impacts, the first is warm waters from the Caribbean do not make it as far into the GOM. This can be seen in the trends composite (Figure 3.2 and Table 3.1) where warming trends in the GOM are lower than the Caribbean.

Examining trends by coral location yields a similar conclusion: SSTAs in the GOM and the Caribbean are varying at different rates with higher rates in the Caribbean. However, each coral record yielded differing warming trends. The main outlier was the Dry Tortugas with a cooling SSTA trend in the GOM in the springtime. However, this cooling trend was nearest in value to the HadISST and ERSST trends surrounding the Dry Tortugas coral location (Figure 3.2). This could be explained by the second impact of the Loop Current and its reduction: eddies that break off the Loop Current in the GOM lead to upwelling and cooler SSTAs in the Dry Tortugas region (Flannery et al., 2024). While cooler SSTAs in this region are apparent, it is not clear if the reduction of the Loop Current would lead to warmer SSTAs in the Dry Tortugas. This warming would be due to a reduction in Loop Current eddies which generate upwelling of cool waters. It is important to note that while the Loop Current appears to be slightly visible as a region of increased warming trends pushing into the GOM (Figure 3.2a), higher-resolution data is needed to better resolve the Loop Current and its eddies.

SST variability in the IAS is complex, and in addition to the Loop Current is impacted by various climate variability patterns. Despite the GOM and the Caribbean's closeness geographically, they do not necessarily vary in the same way or at the same time. In FMA, power spectra analyses indicated significant periodicities in the ranges 4-9 and 21-28 years in the GOM, and 7 and 42 years in the Caribbean. In JJA, significant periodicities in the ranges 4-9 and 16-40 years in the GOM, and 4 and 16-40 years in the Caribbean. NDJ significant periodicities were 4 and 21-28 years in the GOM, and 7 and 42 years in the Caribbean. These results indicate common periodicities between each region and ENSO and PDO. This is supported by Muñoz et al. (2010) who found a positive PNA and a positive PDO lend to cooler SSTAs in the GOM. Though the timescale of PNA is often weeks to months, it is influenced by ENSO and so supports the inclusion of PNA in this discussion. While midlatitude North Pacific climate patterns such as PNA and PDO, more so impact the GOM than the Caribbean, tropical North Pacific patterns such as ENSO, have a greater impact on the Caribbean (Muñoz et al., 2010).

4.2 Springtime Sea Surface Temperature Anomaly Dipole

The variability of SSTAs in the GOM and the Caribbean are directly related to the SSAD. The 1960s saw increased quantity of dipoles across HadISST, ERSST, and coral data as there was a prolonged period of warmer Caribbean SSTAs (Figures 3.10, 3.11, 3.12). The 1960s were marked by mostly neutral ENSO phases and one El Nino. Previous studies determined dipole formation could be due, in part, to strong ENSO events prior to the spring (Muñoz et al., 2010). Muñoz et al. (2010) found warm El

Nino events conducive for dipole formation, however, in this study it appears neutral ENSO phases may also allow for dipole formation (not shown).

With limitations on the scope of data availability further back in time, though improvements in record length were made in this study, it is difficult to determine to what rate the IAS is experiencing an increase or decrease in springtime dipole occurrences. Muñoz et al. (2010) identified the teleconnections that most contribute to the formation of the SSAD and generated a dipole index using March SSTAs. This study incorporated February and April into the dipole calculations as those months are also peak SST difference between the GOM and Caribbean, while also making it more suitable for coral proxy data comparisons. This led to the key result: all data types except for coral records demonstrated the current warming trend inhibits dipole formation. This was seen in Figures 3.10, 3.11, and 3.13 as the average dipoles per decade increased once the linear warming trend was removed. However, with the Caribbean warming faster than the GOM, and a reduction in the Loop Current extent into the GOM, this may not be the case for future decades. Another consideration is needed as cool SSTAs in the GOM and warm SSTAs in the Caribbean must occur concurrently for a dipole to form. An example of this is the cooling trend in the GOM and increased warming trend in the Caribbean during FMA as shown with ERSST. It would be expected to see an increase in the standardized not detrended SSTA dipoles, but in fact, there are less dipoles under these conditions than in HadISST. This is possibly because where those anomalously cool GOM SSTAs occur in time do not line up with the anomalously warm Caribbean. This highlights the need for more in-situ measurements to resolve differences in observational datasets.

4.3 Atlantic Warm Pool

Predictability of the size and intensity of the AWP has beneficial forecasting implications including precipitation and tropical storms. Wang et al. (2008) found that anomalously large AWPs are conducive for tropical storm intensification as they decrease the amount of tropospheric wind shear while also increasing the instability of the troposphere. Figure 3.18 shows the extent of the AWP during dipole years and non-dipole years. The AWP during dipole years extends southeast, further into the Atlantic. Additionally, the region exceeding 28.5℃ (blue contour) is larger during dipole years compared to non-dipole years. There is, however, a region of warmer SSTAs during non-dipole years that extends further into the GOM. This leads to the question of whether certain regions are more impacted by hurricanes during dipole or non-dipole years. For instance, whether this extended warm region, would lead to a more intense hurricane season for the Gulf Coast.

Understanding the importance of AWP impacts, this study explores possible mechanisms that would improve predictability of AWP size and intensity. Though it is widely accepted that ENSO impacts the hydroclimate in the Tropical Atlantic, Wang et al. (2006) found that two-thirds of AWP events were not preceded by a winter El Niño phase. This suggests that while ENSO may impact AWP size and intensity, other mechanisms for AWP development must be examined. The results of this study, however, indicate notable increase in AWP extent and intensity following a SSAD. Thus a greater impact on the summertime AWP may be attributed to a preceding SSAD as opposed to a strong wintertime El Niño. This is further demonstrated in Figures 3.16 and 3.17, as warm SSTAs in the Caribbean persist from FMA into JJA following a SSAD, and cool SSTAs persist following spring seasons without a dipole. However, ENSO must not be understated in its importance, particularly in the formation of a SSAD

through its correlation with Caribbean SSTAs. AWP and connections to SSADs and other climate patterns need to be studied further to improve understanding in drivers of AWP size and intensity.

4.4 Limitations and Future Work

While the utilization of multiple data types can improve the robustness of results and illuminate biases, it also provides added challenges. For instance, each massive coral species required considerations beyond growth rates (Weber, 1973). Amount of light, location of coral colony, symbioticism with zooxanthellae, and coral bleaching alter Sr/Ca ratios and subsequently SST reconstructions (Reynaud et al., 2004). As such, each species has its own Sr/Ca to SST calibration, done by regressing Sr/Ca against SST (Corrège, 2006). Another challenge is the variation of coral sampling, dating, and regression methods across studies. This is particularly challenging when compiling a record across the GOM and the Caribbean which incorporates coral records of different species from different studies. HadISST and ERSST have their own shortcomings: course resolution, and decreased reliability in portions of the records. The extended record length of CESM make it a useful data source, though biases call for careful consideration of results. Using each of these data sources in the same study, however, render the weaknesses of each surmountable.

It is important to address reconstructed SST data limitations as ERSST resolution is coarser than the other data used and has improved reliability after the 1930s (Huang et al., 2017). HadISST, while higher resolution than ERSST, may present a cooling bias since the 1990s (National Center for Atmospheric Research Staff (Eds), 2024). This work would be enhanced by using finer scale data such as NOAA Advanced Very High Resolution Radiometer SST data as well as Optimum Interpolation Sea Surface

Temperature, though with higher resolution, record length is often reduced. While this could be useful for examination of the Loop Current over the past 50 years, it would not be as conducive for long term trends and multi-decadal variability.

This study used the first 10 ensemble members from CESM2 LENS2. LENS2 differs from LENS1 in that it includes both ocean and atmospheric initial states, particularly important for this study as it allows for impacts on SST by AMOC (Rodgers et al., 2021). However, the first 50 members include the un-smoothed biomass burning protocol that was used in the original CMIP6, found to introduce sensitivities impacting the extratropics, though impacts of this discontinuity are still being researched (Rodgers et al., 2021). The biomass burning protocol was smoothed for the second 50 members, removing this discontinuity (Rodgers et al., 2021). For this reason along with the correction of two bugs in the first 50 members involving aerosols and greenhouse gases, future work for this study includes the utilization of all 100 ensemble members for a more apt comparison.

Further, case studies of particularly strong SSADs and mild SSADs would be helpful in determining the type of dipole that contributes to a larger AWP. For instance, would a strong dipole, with cold SSTAs in the GOM inhibit AWP extent as opposed to a mild SSAD with warmer GOM SSTAs? Such case studies would also examine conditions preceding the SSAD (e.g. winter ENSO phase, PNA phase). Understanding the conditions that lead to a strong SSAD allow for better comparison of dipole years per record and provide explanation for years in which all records indicate a dipole occurrences or years in which HadISST, ERSST, coral reconstructions, and CESM are in disagreement.

This work has demonstrated the importance of utilizing available paleoproxy data. The fourth objective of this study was to increase data record length and compare results across multiple datasets. There is more work to be done towards this goal

including adding more coral sites in the IAS and extending coral records further back in time. Work is being done to reconstruct SST from corals near the Yucatan and Haiti, improving the distribution of available data in the IAS, leading to results more representative of each region as a whole. This study and future work mentioned above, provide evidence of the benefits of and support for the use of paleoclimate data across disciplines.

Chapter 5

Conclusions

Observations, coral proxy data, and the first ten ensemble members of CESM2 LENS2 were used to examine the climate variability in the IAS by comparing SST variability between the GOM and Caribbean, analyzing the SSAD and its potential drivers, and evaluating the relation between the SSAD and the AWP with the goal of providing useful information to improve predictability of phenomena attributed to impacting severe weather (e.g. hurricanes).

While there was some discrepancy to the degree at which the IAS is warming, all records indicated enhanced warming of the Caribbean compared to the GOM. This has direct implications for the SSAD, as removing the warming trend led to decreased dipole occurrences. In other words, the warming trend inhibits dipole formation. However, as the Caribbean warms faster than the GOM, a threshold could be reached where there is an increase in SSAD occurrences in future decades. If this were the case, it could mean increased precipitation along the southeast and west coast of the United States with annomlaously dry conditions enhanced in the Amazon Basin, midwest, and northeast United States.

As the AWP had increased extent and intensity following a SSAD than when a dipole was not present the preceding spring, understanding of climate patterns contributing to the formation of SSADs are of particular importance. Significant periodicities in each region were found to match ENSO (and subsequently PNA), and the PDO. Understanding the mechanisms driving these potential relationships between

SST variability, IAS phenomena (SSAD and AWP), and climate patterns are critical for hydroclimate predictions in the IAS.

Increased record length and the use of multiple data types improves reliability of results and illuminates biases in data that is often used in climate predictions or at least in comparison to predictions. For instance, annual CESM trends in the Caribbean were an order of magnitude smaller than ERSST and HadISST, and an order of magnitude smaller than coral trends in FMA. Considering the broader impacts of these phenomena on hydroclimate, this work can contribute to a better understanding of SST variability in the GOM and Caribbean that results in their development and, in turn improving predictive skill of these phenomena.

This study is the culmination of interdisciplinary work between atmospheric science and paleoclimatology and illustrates the benefits of using atmospheric data and paleoproxies in combination. These benefits include increased record length, volume of available data, range of climate parameters derived, and ability to compare results, improving reliability. As mentioned previously, GCMs contain biases that impact reliability of results. By incorporating coral proxy data with observations and models, not only can record length reach further into the past, but comparisons lead to improved reliability, opening a potential avenue for model evaluation in future work.

Reference List

Brocas, W. M., T. Felis, J. C. Obert, P. Gierz, G. Lohmann, D. Scholz, M. Kölling, and S. R. Scheffers, 2016: Last interglacial temperature seasonality reconstructed from tropical atlantic corals. *Earth and Planetary Science Letters*, **449**, 418–429, https://doi.org/https://doi.org/10.1016/j.epsl.2016.06.005.

Brotons, M., R. Haarsma, N. Bloemendaal, H. de Vries, and T. Allen, 2024: Drivers of caribbean precipitation change due to global warming: analyses and emergent constraint of cmip6 simulations. *Climate Dynamics*, **62 (5)**, 3395–3415, https://doi.org/10.1007/s00382-023-07072-3.

Buddemeier, R. W., J. E. Maragos, and D. W. Knutson, 1974: Radiographic studies of reef coral exoskeletons: Rates and patterns of coral growth. *Journal of Experimental Marine Biology and Ecology*, **14 (2)**, 179–199, https://doi.org/https://doi.org/10.1016/0022-0981(74)90024-0.

Corrège, T., 2006: Sea surface temperature and salinity reconstruction from coral geochemical tracers. *Palaeogeography, Palaeoclimatology, Palaeoecology*, **232 (2)**, 408–428, https://doi.org/https://doi.org/10.1016/j.palaeo.2005.10.014.

DeLong, K. L., J. A. Flannery, C. R. Maupin, R. Z. Poore, and T. M. Quinn, 2011: A coral sr/ca calibration and replication study of two massive corals from the gulf of mexico. *Palaeogeography, Palaeoclimatology, Palaeoecology*, **307 (1)**, 117–128, https://doi.org/https://doi.org/10.1016/j.palaeo.2011.05.005.

DeLong, K. L., J. A. Flannery, R. Z. Poore, T. M. Quinn, C. R. Maupin, K. Lin, and C.-C. Shen, 2014: A reconstruction of sea surface temperature variability in the southeastern gulf of mexico from 1734 to 2008 c.e. using cross-dated sr/ca records from the coral siderastrea siderea. *Paleoceanography*, **29 (5)**, 403–422, https://doi.org/https://doi.org/10.1002/2013PA002524.

DeLong, K. L., C. R. Maupin, J. A. Flannery, T. M. Quinn, and C.-C. Shen, 2016: Refining temperature reconstructions with the atlantic coral siderastrea siderea. *Palaeogeography, Palaeoclimatology, Palaeoecology*, **462**, 1–15, https://doi.org/https://doi.org/10.1016/j.palaeo.2016.08.028.

Deser, C., M. A. Alexander, and M. S. Timlin, 2003: Understanding the persistence of sea surface temperature anomalies in midlatitudes. *Journal of Climate*, **16 (1)**, 57–72, https://doi.org/10.1175/1520-0442(2003)016⟨0057:UTPOSS⟩2.0.CO;2.

Duan, X., F. Xue, and F. Zheng, 2021: Sea surface temperature anomaly in the tropical north atlantic during el niño decaying years. *Atmospheric and Oceanic Science Letters*, **14 (6)**, 100 077, https://doi.org/https://doi.org/10.1016/j.aosl.2021.100077.

Durán-Quesada, A. M., R. Sorí, P. Ordoñez, and L. Gimeno, 2020: Climate perspectives in the intra–americas seas. *Atmosphere*, **11 (9)**, https://doi.org/10.3390/atmos11090959, URL https://www.mdpi.com/2073-4433/11/9/959.

Enfield, D. B., S.-K. Lee, and C. Wang, 2006: How are large western hemisphere warm pools formed? *Progress in Oceanography*, **70 (2)**, 346–365, https://doi.org/https://doi.org/10.1016/j.pocean.2005.07.006.

Flanders Marine Institute, 2018: Iho sea areas, version 3. URL https://www.marineregions.org/, https://doi.org/10.14284/323.

Flannery, J., and R. Poore, 2013: Sr/ca proxy sea-surface temperature reconstructions from modern and holocene montastraea faveolata specimens from the dry tortugas national park, florida, u.s.a. *Journal of Coastal Research*, **63**, 20–31, https://doi.org/10.2307/23486500.

Flannery, J. A., J. N. Richey, K. Thirumalai, R. Z. Poore, and K. L. DeLong, 2017: Multi-species coral sr/ca-based sea-surface temperature reconstruction using orbicella faveolata and siderastrea siderea from the florida straits. *Palaeogeography, Palaeoclimatology, Palaeoecology*, **466**, 100–109, https://doi.org/https://doi.org/10.1016/j.palaeo.2016.10.022.

Flannery, J. A., J. N. Richey, L. T. Toth, I. B. Kuffner, and R. Z. Poore, 2018: Quantifying uncertainty in sr/ca-based estimates of sst from the coral orbicella faveolata. *Paleoceanography and Paleoclimatology*, **33 (9)**, 958–973, https://doi.org/https://doi.org/10.1029/2018PA003389.

Flannery, J. A., J. N. Richey, L. T. Toth, and M. J. Mette, 2024: 20th century warming in the western florida keys was dominated by increasing winter temperatures. *Paleoceanography and Paleoclimatology*, **39 (2)**, e2023PA004748, https://doi.org/https://doi.org/10.1029/2023PA004748.

Glenn, E., D. Comarazamy, J. E. González, and T. Smith, 2015: Detection of recent regional sea surface temperature warming in the caribbean and surrounding region. *Geophysical Research Letters*, **42 (16)**, 6785–6792, https://doi.org/https://doi.org/10.1002/2015GL065002.

González, J., M. Georgescu, M. Lemos, N. Hosannah, and D. Niyogi, 2017: Climate change's pulse is in central america and the caribbean. *Eos*, **98**, https://doi.org/https://doi.org/10.1029/2017EO071975.

Harbott, M., H. C. Wu, H. Kuhnert, C. Jimenez, P. González-Díaz, and T. Rixen, 2023: Stable isotope and trace element data for a siderastrea siderea coral core cim_c_2-2-1/cim_c_2-2-2 from the gulf of mexico. *PANGAEA*, https://doi.org/10.1594/PANGAEA.963278, URL https://doi.org/10.1594/PANGAEA.963278.

Hetzinger, S., M. Pfeiffer, W.-C. Dullo, D. Garbe-Schönberg, and J. Halfar, 2010: Rapid 20th century warming in the caribbean and impact of remote forcing on climate in the northern tropical atlantic as recorded in a guadeloupe coral. *Palaeogeography, Palaeoclimatology, Palaeoecology*, **296 (1)**, 111–124, https://doi.org/https://doi.org/10.1016/j.palaeo.2010.06.019.

Hetzinger, S., M. Pfeiffer, W.-C. Dullo, E. Ruprecht, and D. Garbe-Schönberg, 2006: Sr/ca and 18o in a fast-growing diploria strigosa coral: Evaluation of a new climate archive for the tropical atlantic. *Geochemistry, Geophysics, Geosystems*, **7 (10)**, https://doi.org/https://doi.org/10.1029/2006GC001347, URL https://agupubs.onlinelibrary.wiley.com/doi/abs/10.1029/2006GC001347.

Hickey, D., C. Reich, K. DeLong, R. Poore, and J. Brock, 2013: *Holocene core logs and site methods for modern reef and head-coral cores: Dry Tortugas National Park, Florida*. U.S. Geological Survey.

Huang, B., and Coauthors, 2017: Extended reconstructed sea surface temperature, version 5 (ersstv5): Upgrades, validations, and intercomparisons. *Journal of Climate*, **30 (20)**, 8179–8205, https://doi.org/10.1175/JCLI-D-16-0836.1.

Liu, Y., S.-K. Lee, B. A. Muhling, J. T. Lamkin, and D. B. Enfield, 2012: Significant reduction of the loop current in the 21st century and its impact on the gulf of mexico. *Journal of Geophysical Research: Oceans*, **117 (C5)**, https://doi.org/https://doi.org/10.1029/2011JC007555, URL https://agupubs.onlinelibrary.wiley.com/doi/abs/10.1029/2011JC007555.

Manzello, D. P., 2015: Rapid recent warming of coral reefs in the florida keys. *Scientific Reports*, **5 (1)**, 16 762, https://doi.org/10.1038/srep16762.

Martin, E. R., and C. Schumacher, 2012: The relationship between tropical warm pool precipitation, sea surface temperature, and large-scale vertical motion in ipcc ar4 models. *Journal of the Atmospheric Sciences*, **69 (1)**, 185–194, https://doi.org/10.1175/JAS-D-11-0104.1.

Muñoz, E., C. Wang, and D. Enfield, 2010: The intra-americas springtime sea surface temperature anomaly dipole as fingerprint of remote influences. *Journal of Climate*, **23 (1)**, 43–56, https://doi.org/https://doi.org/10.1175/2009JCLI3006.1.

National Center for Atmospheric Research Staff (Eds), 2024: The climate data guide: Sst data: Hadisst v1.1. URL https://climatedataguide.ucar.edu/climate-data/sst-data-hadisst-v11.

Ong, M. R., N. F. Goodkin, R. Guppy, and K. A. Hughen, 2022: Colpophyllia natans from tobago, a novel paleoclimate archive for reconstructing sea surface temperature in the tropical atlantic. *Paleoceanography and Paleoclimatology*,

37 (12), e2022PA004 483, https://doi.org/https://doi.org/10.1029/2022PA004483, URL https://agupubs.onlinelibrary.wiley.com/doi/abs/10.1029/2022PA004483.

Rayner, N., and Coauthors, 2003: Global analyses of sea surface temperature, sea ice, and night marine air temperature since the late nineteenth century. *J. Geophys. Res.*, **108 (D14)**, 4407, https://doi.org/https://doi.org/10.1029/2002JD002670.

Reynaud, S., C. Ferrier-Pagès, F. Boisson, D. Allemand, and R. G. Fairbanks, 2004: Effect of light and temperature on calcification and strontium uptake in the scleractinian coral acropora verweyi. *Marine Ecology Progress Series*, **279**, 105–112.

Rodgers, K. B., and Coauthors, 2021: Ubiquity of human-induced changes in climate variability. *Earth System Dynamics*, **12 (4)**, 1393–1411, https://doi.org/10.5194/esd-12-1393-2021, URL https://esd.copernicus.org/articles/12/1393/2021/.

von Reumont, J., S. Hetzinger, D. Garbe-Schönberg, C. Manfrino, and C. Dullo, 2018: Tracking interannual- to multidecadal-scale climate variability in the atlantic warm pool using central caribbean coral data. *Paleoceanography and Paleoclimatology*, **33 (4)**, 395–411, https://doi.org/https://doi.org/10.1002/2018PA003321.

von Reumont, J., S. Hetzinger, D. Garbe-Schönberg, C. Manfrino, and W.-C. Dullo, 2016: Impact of warming events on reef-scale temperature variability as captured in two little cayman coral sr/ca records. *Geochemistry, Geophysics, Geosystems*, **17 (3)**, 846–857, https://doi.org/https://doi.org/10.1002/2015GC006194.

Walter, R. M., and Coauthors, 2023: The CoralHydro2k database: a global, actively curated compilation of coral ^{18} O and Sr Ca proxy records of tropical ocean hydrology and temperature for the Common Era. *Earth System Science Data*, **15 (5)**, 2081–2116, https://doi.org/10.5194/essd-15-2081-2023, URL https://essd.copernicus.org/articles/15/2081/2023/.

Wang, C., and D. B. Enfield, 2001: The tropical western hemisphere warm pool. *Geophysical Research Letters*, **28 (8)**, 1635–1638, https://doi.org/https://doi.org/10.1029/2000GL011763.

Wang, C., D. B. Enfield, S.-k. Lee, and C. W. Landsea, 2006: Influences of the atlantic warm pool on western hemisphere summer rainfall and atlantic hurricanes. *Journal of Climate*, **19 (12)**, 3011–3028, https://doi.org/10.1175/JCLI3770.1.

Wang, C., S.-k. Lee, and D. B. Enfield, 2007: Impact of the atlantic warm pool on the summer climate of the western hemisphere. *Journal of Climate*, **20 (20)**, 5021–5040, https://doi.org/10.1175/JCLI4304.1.

Wang, C., S.-K. Lee, and D. B. Enfield, 2008: Climate response to anomalously large and small atlantic warm pools during the summer. *Journal of Climate*, **21 (11)**, 2437–2450, https://doi.org/https://doi.org/10.1175/2007JCLI2029.1.

Weber, J. N., 1973: Incorporation of strontium into reef coral skeletal carbonate. *Geochimica et Cosmochimica Acta*, **37 (9)**, 2173–2190, https://doi.org/https://doi.org/10.1016/0016-7037(73)90015-X.

Weinzierl, M. S., C. D. Reich, T. D. Hickey, L. A. Bartlett, and I. B. Kuffner, 2016: *Collection methods and descriptions of coral cores extracted from massive corals in Dry Tortugas National Park, Florida, U.S.A.* No. 2016–1182, Open-File Report, Reston, VA, https://doi.org/10.3133/ofr20161182, URL https://pubs.usgs.gov/publication/ofr20161182.

Xu, Z., F. Ji, B. Liu, T. Feng, Y. Gao, Y. He, and F. Chang, 2021: Long-term evolution of global sea surface temperature trend. *International Journal of Climatology*, **41 (9)**, 4494–4508, https://doi.org/https://doi.org/10.1002/joc.7082.

1 Appendix A

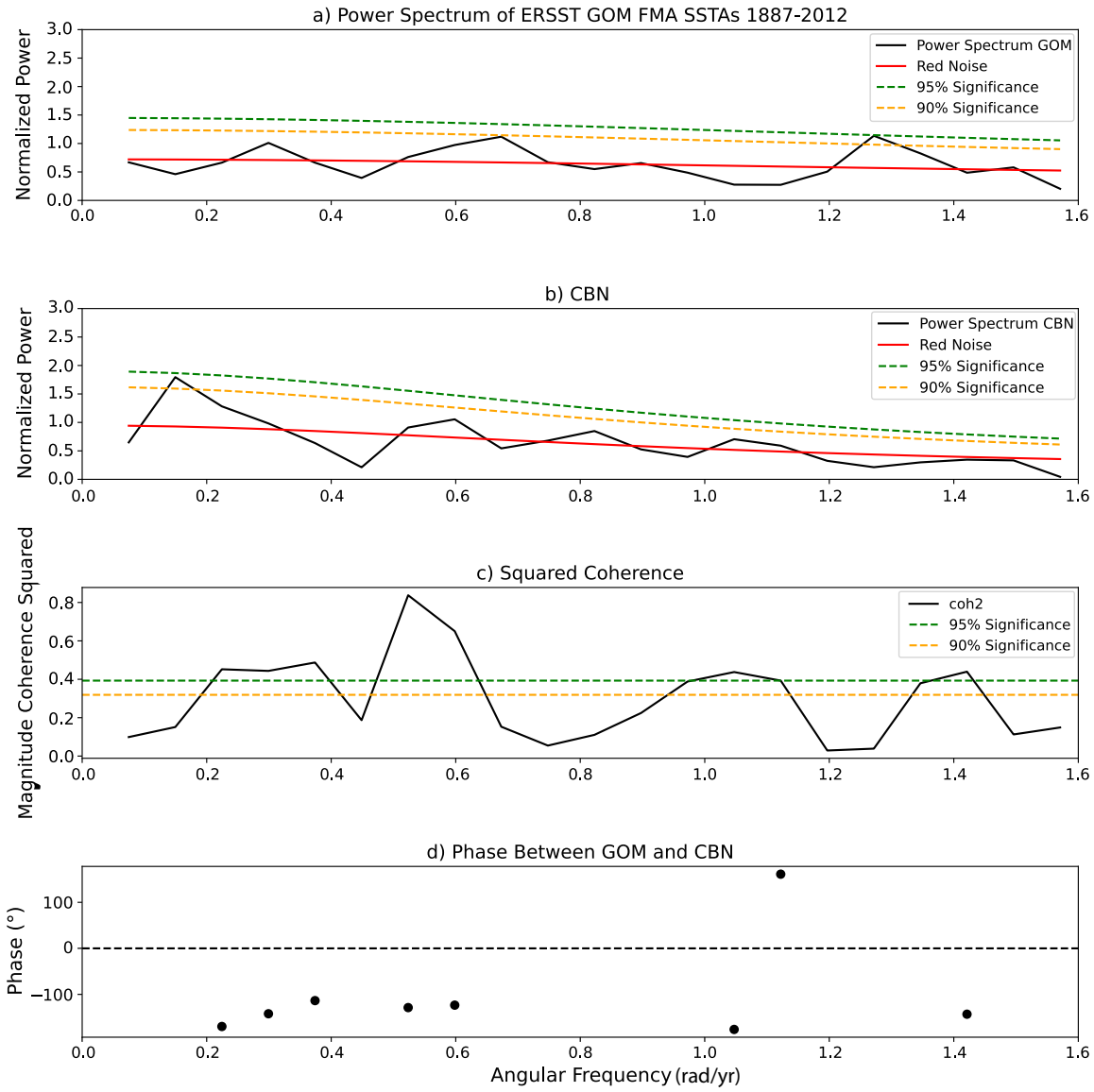


Figure A.1: Spectral analysis of area-averaged, detrended, standardized SSTAs using ERSST for the (a) GOM and (b) Caribbean during FMA from 1887-2012. In panels a-b, the SSTAs (black-solid), red noise (red-solid), 95% (green-dahsed) and 90% (orange) significance are shown. (c) Coherence squared between the GOM and Caribbean time series shown with 95% and 90% significance. (d) Phase relationship between the time series, only shown when coherence squared is significant at 95%. Phase difference is zero at the dashed line.

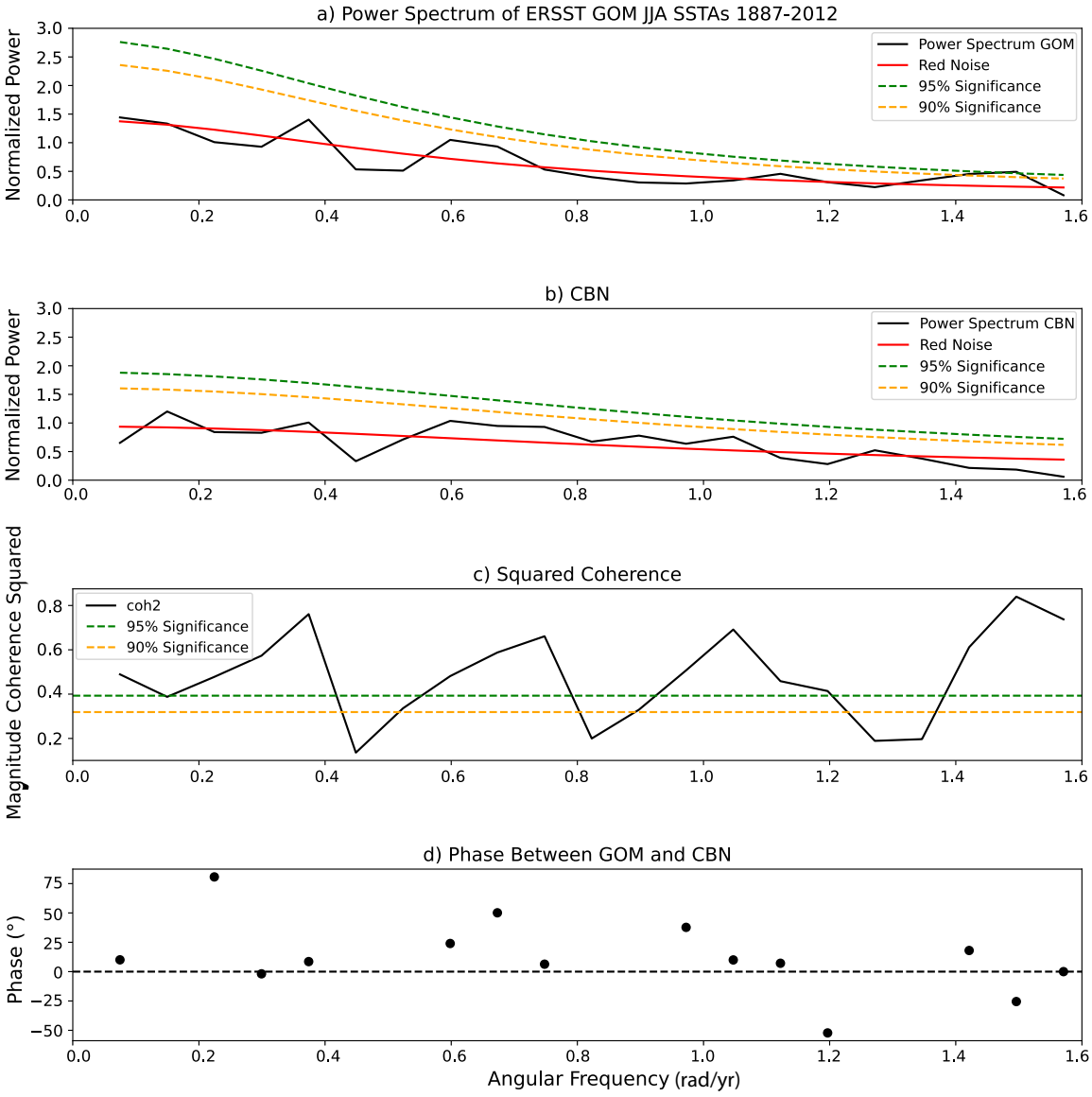


Figure A.2: Spectral analysis of area-averaged, detrended, standardized SSTAs using ERSST for the (a) GOM and (b) Caribbean during JJA from 1887-2012. In panels a-b, the SSTAs (black-solid), red noise (red-solid), 95% (green-dahsed) and 90% (orange) significance are shown. (c) Coherence squared between the GOM and Caribbean time series shown with 95% and 90% significance. (d) Phase relationship between the time series, only shown when coherence squared is significant at 95%. Phase difference is zero at the dashed line.

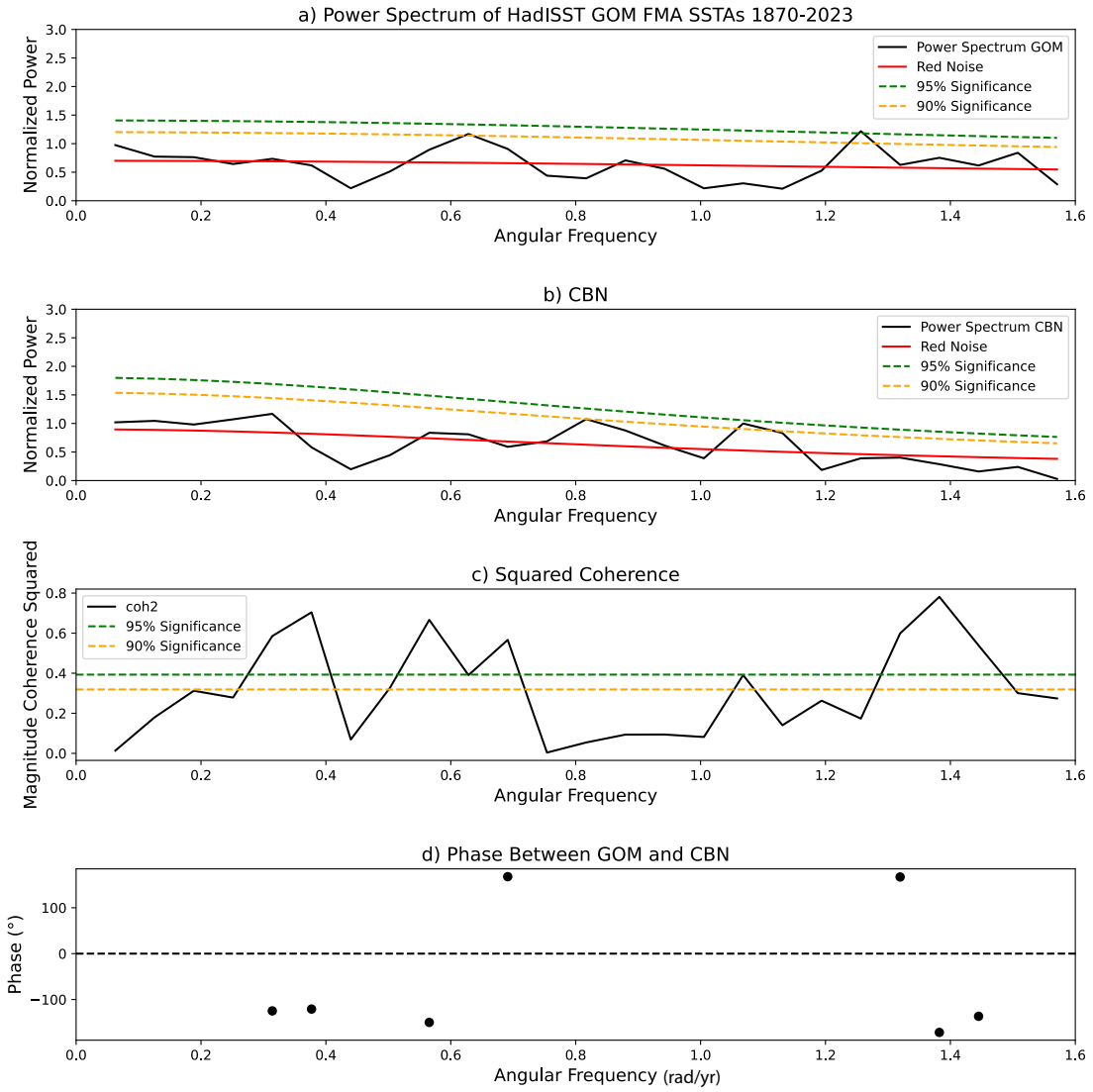


Figure A.3: Spectral analysis of area-averaged, detrended, standardized SSTAs using HadISST for the (a) GOM and (b) Caribbean during FMA from 1870-2023. In panels a-b, the SSTAs (black-solid), red noise (red-solid), 95% (green-dahsed) and 90% (orange) significance are shown. (c) Coherence squared between the GOM and Caribbean time series shown with 95% and 90% significance. (d) Phase relationship between the time series, only shown when coherence squared is significant at 95%. Phase difference is zero at the dashed line.

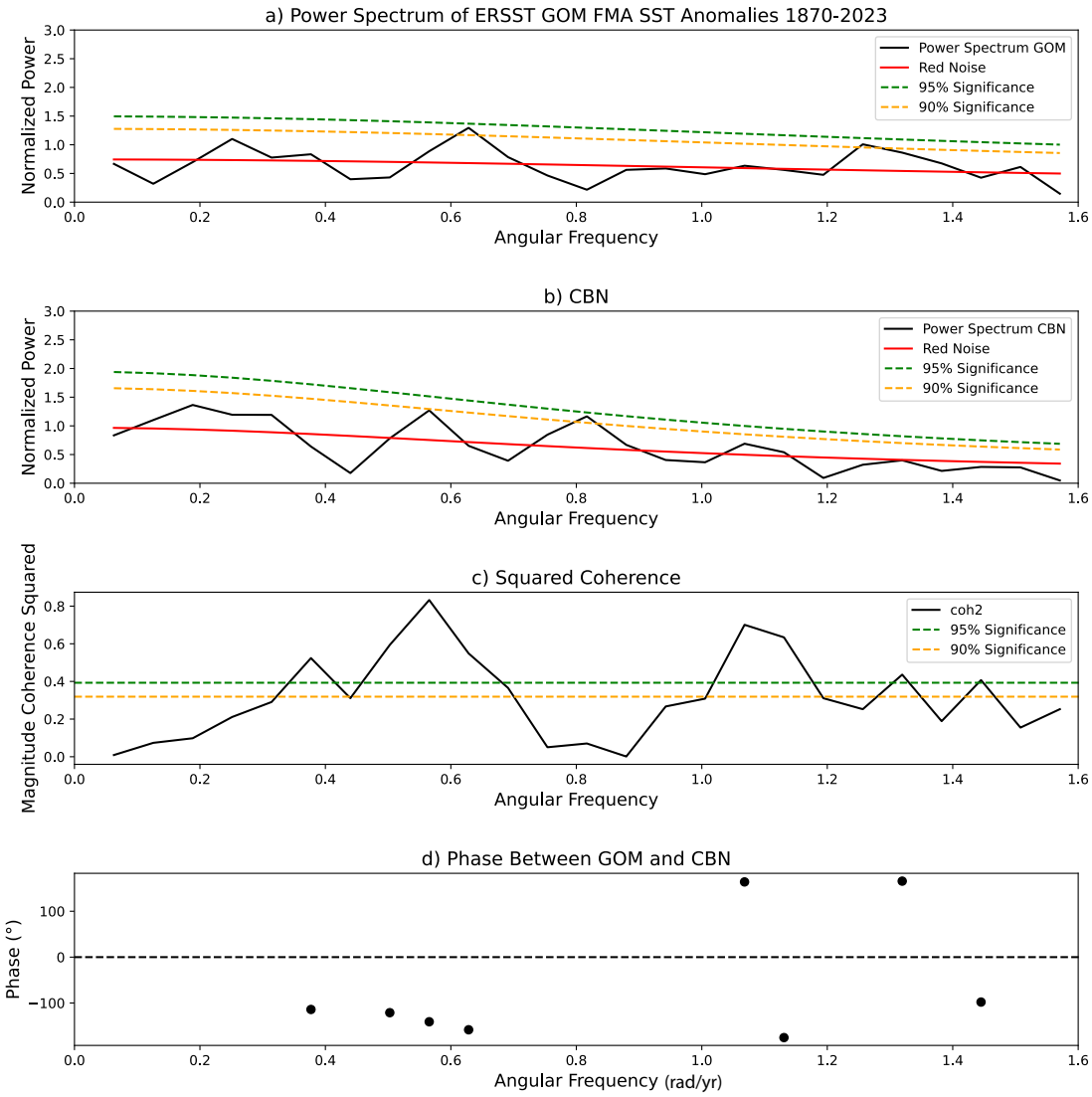


Figure A.4: Same as Figure A.1 except with ERSST.

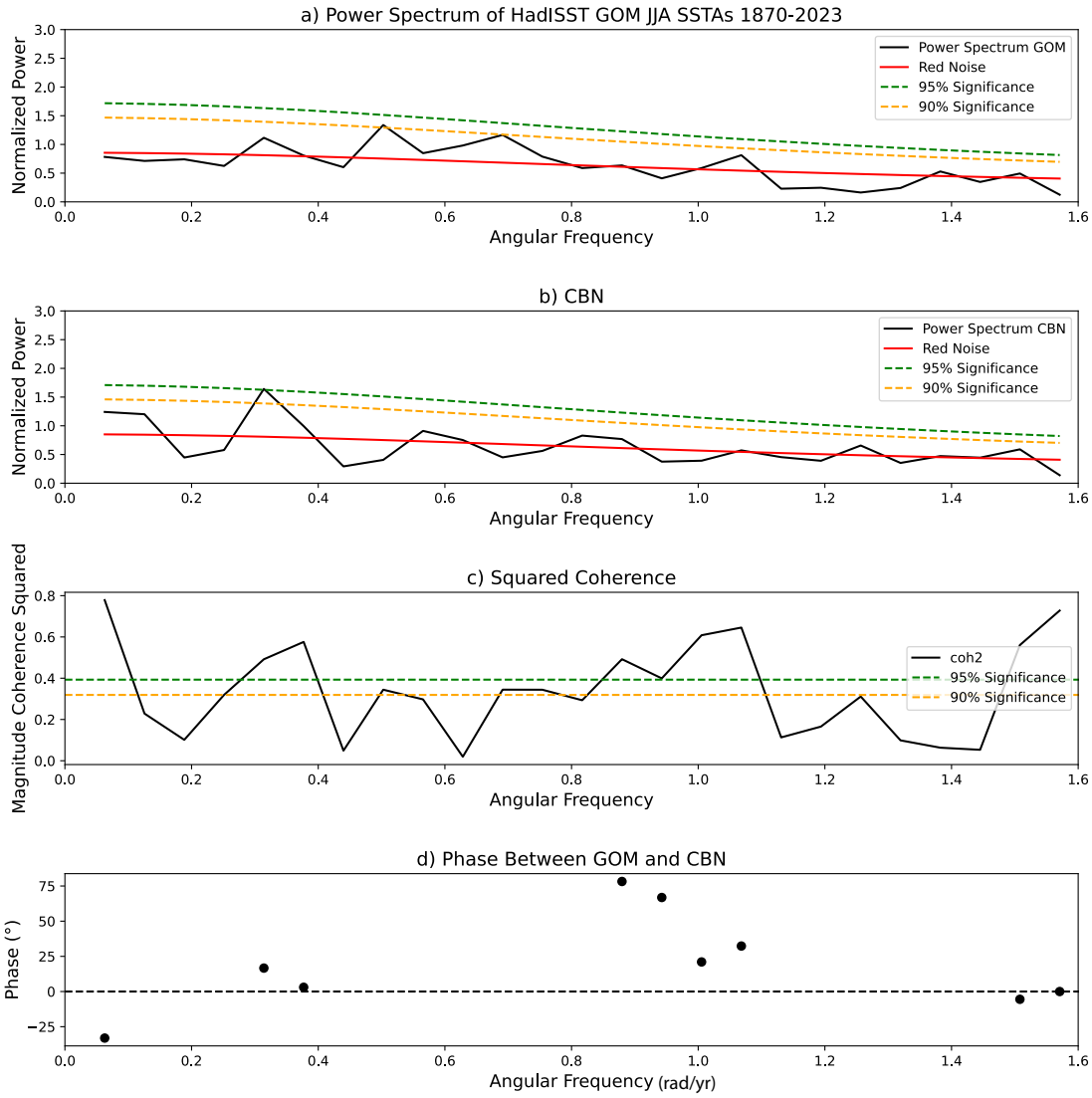


Figure A.5: Spectral analysis of area-averaged, detrended, standardized SSTAs using HadISST for the (a) GOM and (b) Caribbean during JJA from 1870-2023. In panels a-b, the SSTAs (black-solid), red noise (red-solid), 95% (green-dahsed) and 90% (orange) significance are shown. (c) Coherence squared between the GOM and Caribbean time series shown with 95% and 90% significance. (d) Phase relationship between the time series, only shown when coherence squared is significant at 95%. Phase difference is zero at the dashed line.

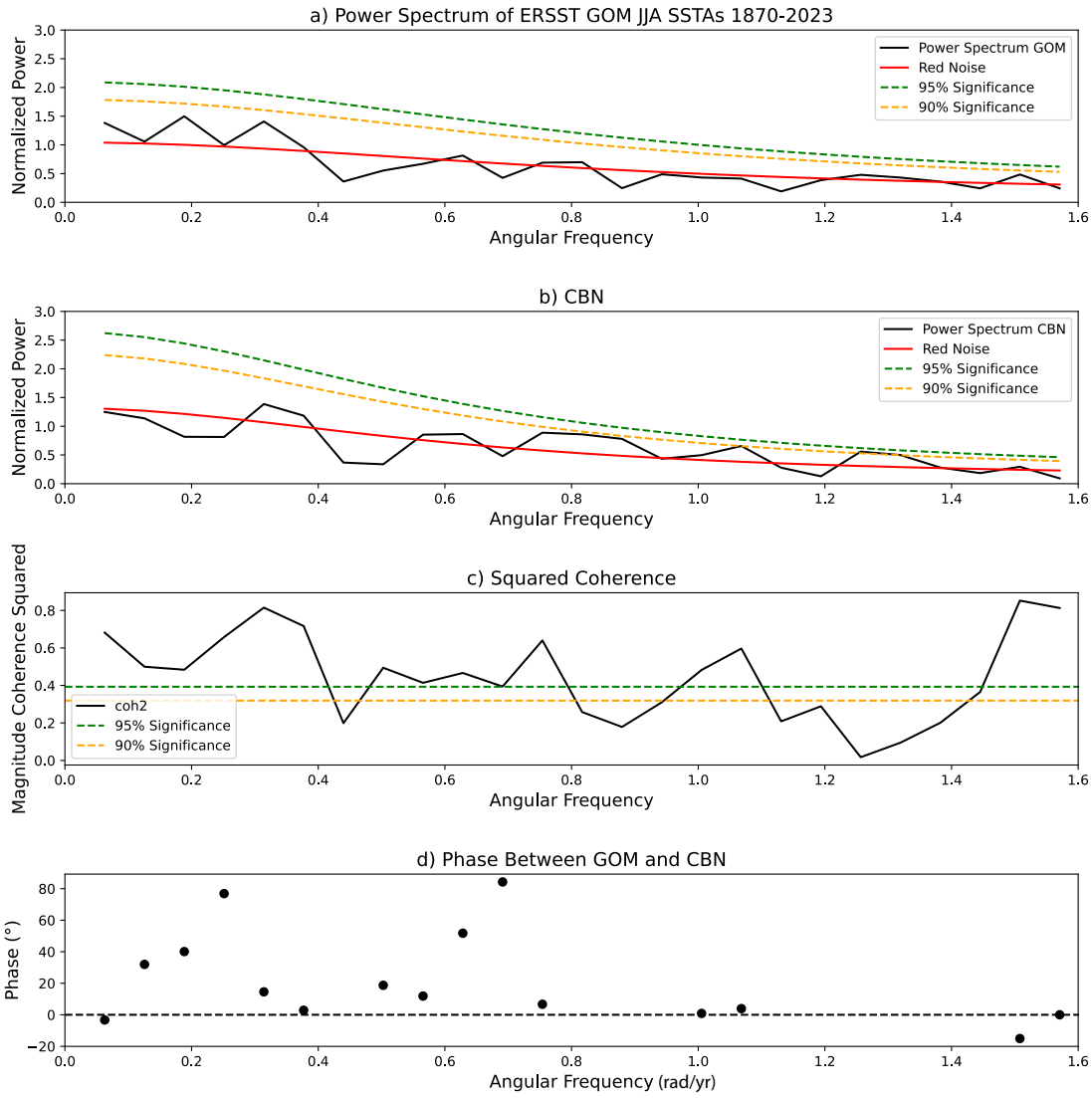


Figure A.6: Same as Figure A.3 except with ERSST.

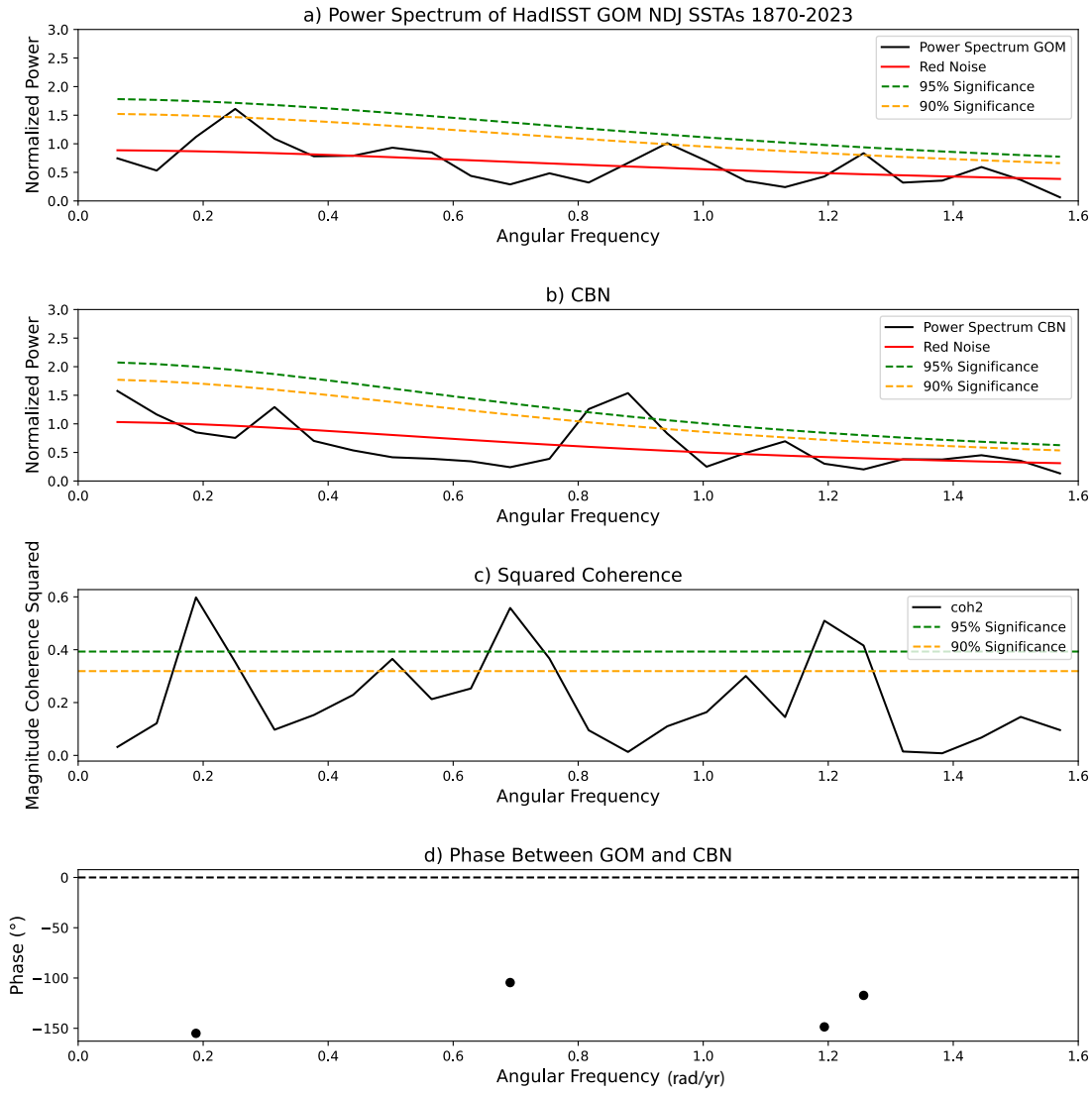


Figure A.7: Spectral analysis of area-averaged, detrended, standardized SSTAs using HadISST for the (a) GOM and (b) Caribbean during NDJ from 1870-2023. In panels a-b, the SSTAs (black-solid), red noise (red-solid), 95% (green-dahsed) and 90% (orange) significance are shown. (c) Coherence squared between the GOM and Caribbean time series shown with 95% and 90% significance. (d) Phase relationship between the time series, only shown when coherence squared is significant at 95%. Phase difference is zero at the dashed line.

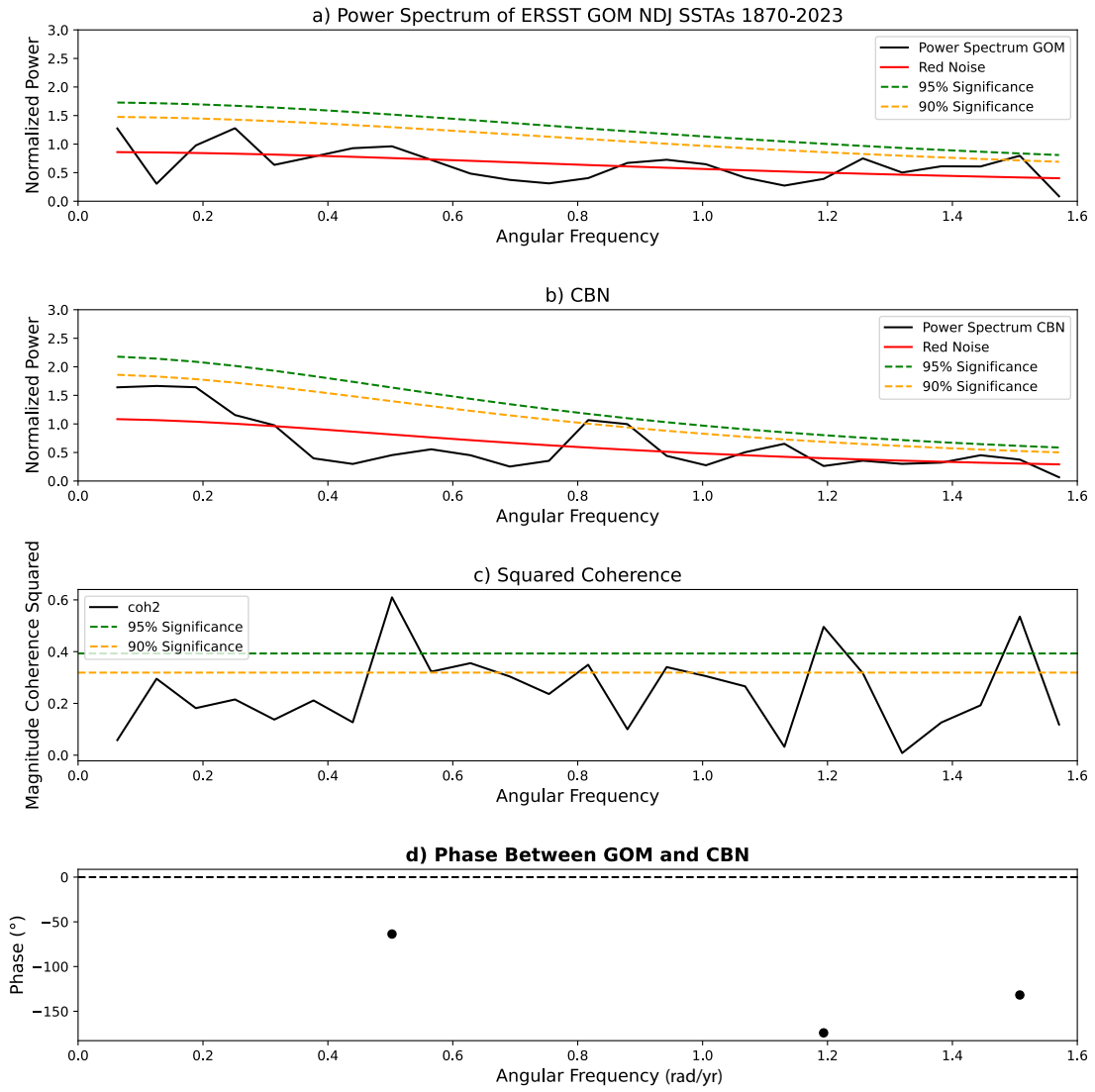


Figure A.8: Same as Figure A.5 except with ERSST.

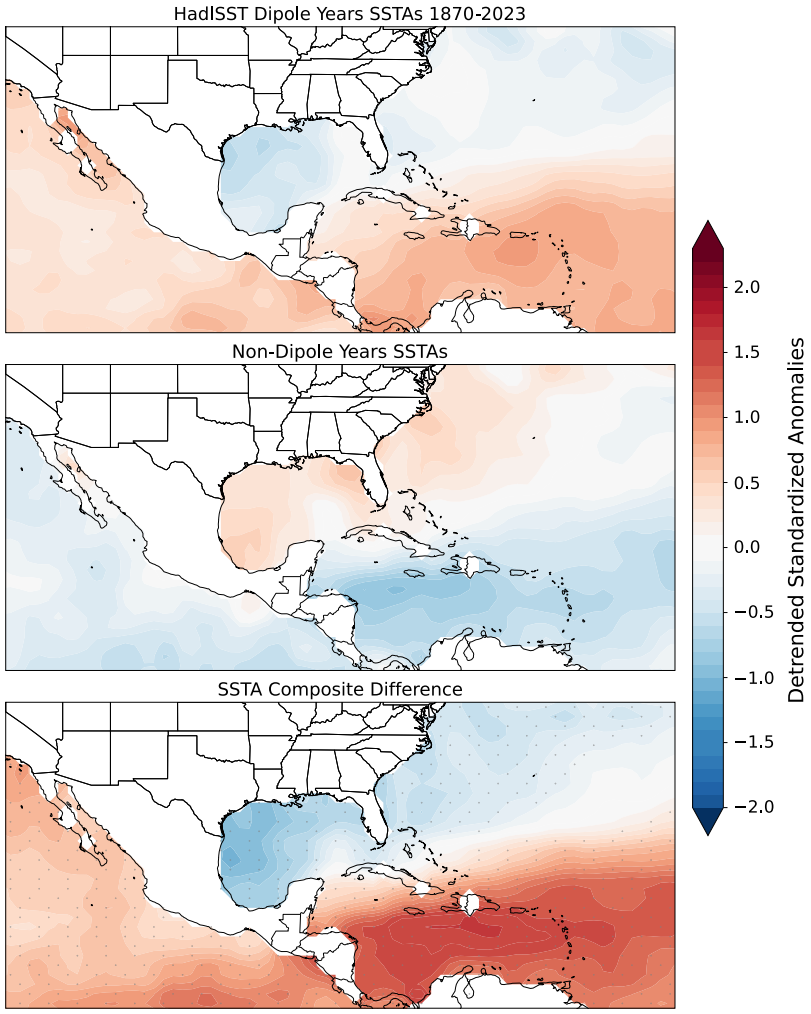


Figure A.9: Composite of detrended standardized SSTAs in the IAS using HadISST from 1870-2023 during (top) dipole years, (middle) non-dipole years, and (bottom) composite difference with 99% confidence (gray dots) using a Monte Carlo test.

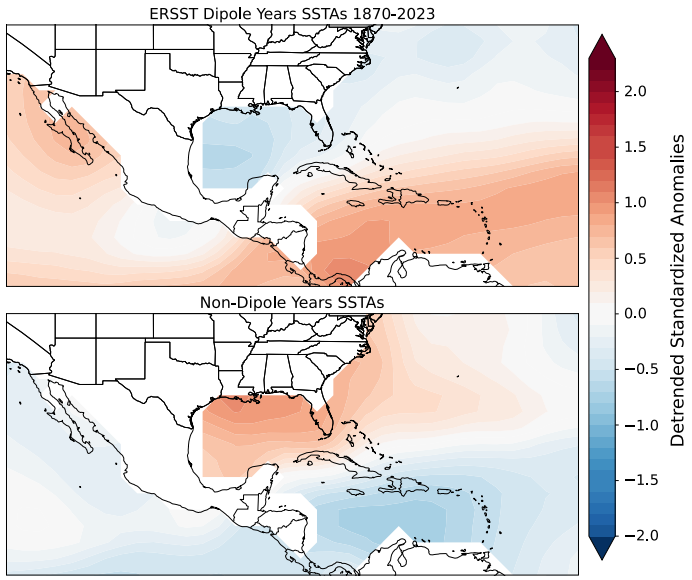


Figure A.10: Composite of detrended standardized SSTAs in the IAS using ERSST from 1870-2023 during (top) dipole years, and (bottom) non-dipole years.

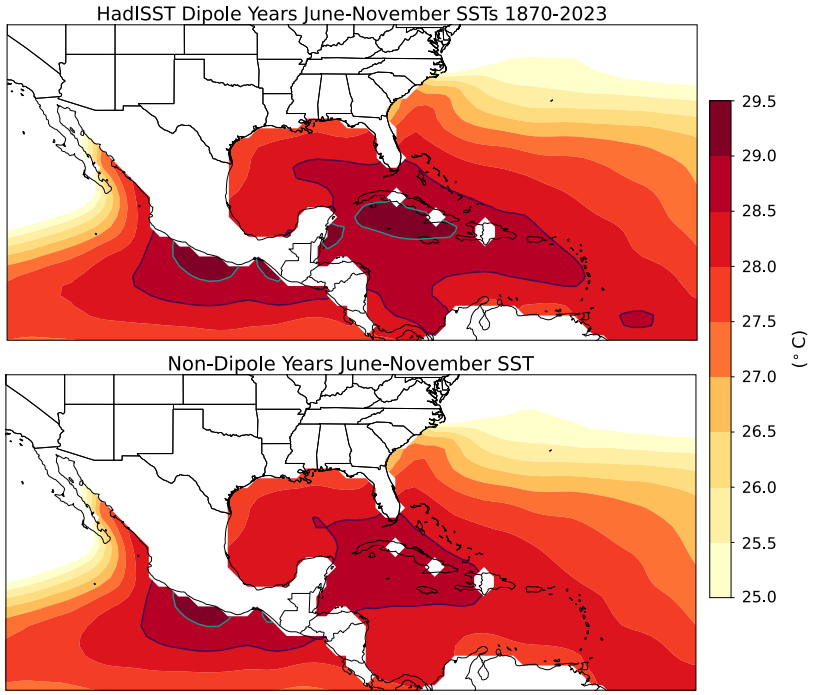


Figure A.11: Composite of hurricane season-mean SSTs in the IAS using HadISST during (top) dipole years, and (bottom) non-dipole years. Black contour at 28.5℃ and blue contour at 29.5℃.

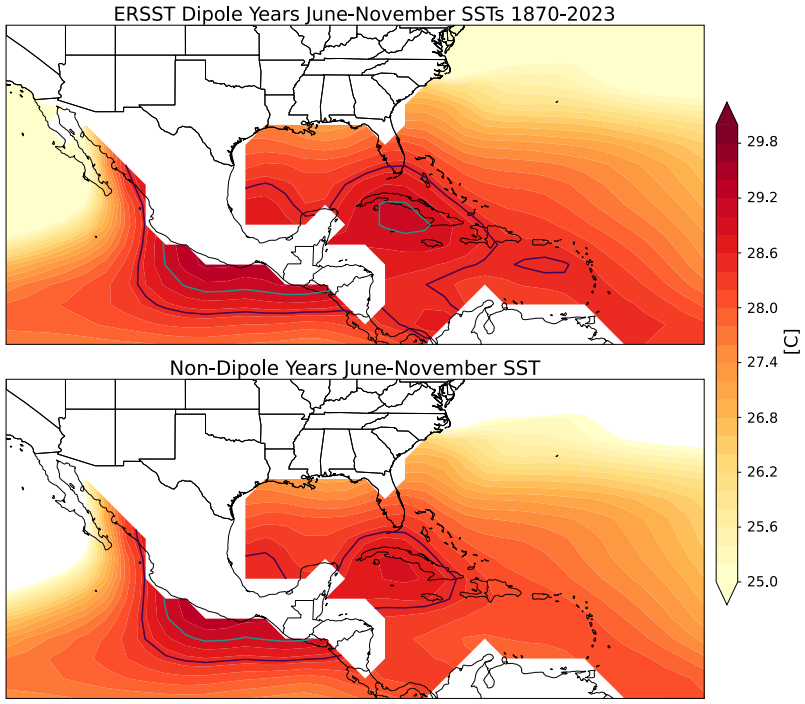


Figure A.12: Composite of hurricane season-mean SSTs in the IAS using ERSST during (top) dipole years, and (bottom) non-dipole years. Black contour at 28.5℃ and blue contour at 29.5℃.